Photovoltaic Effect

RICHARD H. BUBE AND ALAN L. FAHRENBRUCH

Department of Materials Science and Engineering
Stanford University
Stanford, California

I. Introduction 163
II. An Overview of Photovoltaic Effects 166
A. Types of Semiconductor Junctions 166
B. Simple Photovoltaic Cell Model 171
C. More General Photovoltaic Cell Model 174
D. Major Processes and Mechanisms 179
III. Current Generation 189
A. Derivation of the Transport Equation 190
B. Solution of the Transport Equation 191
C. Other Contributions to Current Generation 193
IV. Junction Currents 193
A. Homojunctions 193
B. Heterojunctions 194
C. Schottky Barriers 198
D. MIS Junctions 198
E. SIS Junctions 200
V. Examples of Photovoltaic Materials Systems 200
A. Silicon 201
B. Gallium Arsenide 204
C. Cu_xS/CdS Thin-Film Heterojunctions 206
D. Indium Phosphide 208
E. Cadmium Telluride 209
F. $CuInSe_2$ 209
G. Other Possible Materials of Promise 210
References 211

I. INTRODUCTION

The photovoltaic effect is one of several fundamental photoeffects involving the interaction of light with solid state materials. Other related effects are photoconductivity, photoluminescence, and photoemission. In photoconductivity, the absorption of light that increases the density of free carriers in a material with an applied electric field results in an increase in conductivity. In photoluminescence, the absorption of light that raises electrons to excited states, either free or localized, results in the emission of luminescence when these excited electrons return to their ground state with

Copyright © 1981 by Academic Press, Inc.
All rights of reproduction in any form reserved.
ISBN 0-12-014656-8

the release of their energy as light. In photoemission, the absorption of light that creates free carriers with sufficient energy to pass over a surface or interface barrier results in the emission of electrons from the material into a vacuum (external photoemission) or into a second material (internal photoemission) All three of these phenomena may be observed with only homogeneous materials (although, of course, they may also occur in materials containing internal junction fields), but the photovoltaic effect requires an internal junction field in the material for its observation. The photovoltaic effect is therefore most often associated with the presence of junctions in semiconductor materials, which act to separate the carriers generated by absorption of light in order to produce a conversion of the power from the absorbed light into electric power. In many ways the process of photovoltaic power generation can be thought of as the inverse of the process of electroluminescence; in electroluminescence an applied electric field that forward-biases a semiconductor junction leads to the generation of luminescence emission, whereas in the photovoltaic effect, absorption of radiation leads to the generation of an electric field, in all but a short-circuit configuration.

The photovoltaic effect received relatively little general attention for many years after its initial discovery in the midnineteenth century. The actual origin of the effect should probably be traced back to the work of Becquerel (*1*), who in 1839 discovered that shining a light on an electrode in an electrolyte solution led to the generation of a photovoltage. Forty years later Adams and Day (*2*) observed a similar effect in the solid material selenium, within a few years of the date that Willoughby Smith discovered photoconductivity in this material (*3*). For many years only selenium and cuprous oxide were known to give rise to the effect, and it was not until about 1914 that it was realized that an energy barrier was involved in both types of cell. The selenium photovoltaic cell was used for photographic exposure meters and achieved a conversion efficiency of about 1% for solar radiation. The conversion efficiency of a photovoltaic device is expressed as the ratio of the maximum power generated by the cell to the total radiation power incident on the cell.

The outbreak of interest in the space program with the application of photovoltaic cells to power space vehicles gave a fresh impetus to research on photovoltaics. Single crystal silicon was the first material used; in 1954 a solar conversion efficiency of 6% had been reported (*4*), which was rapidly increased to 14% within four years. Another single crystal cell based on gallium arsenide was reported to have an efficiency of 4% in 1956 (*5*), and the efficiency of this cell has since been increased to 24% by taking advantage of new technology. Although space applications did not have cost considerations as a primary factor, they did have concerns for weight and flexibility; these considerations led to the investigation of thin-film photovoltaic cells.

The cuprous sulfide–cadmium sulfide heterojunction cell, first reported with an efficiency of 6% in 1954 (*6*), has had its efficiency increased by concentrated research to over 9% in 1980 (*7*).

Photovoltaic research suffered a hiatus when the space program ceased to have top priority. Within a few years, however, the realization of the need for new energy sources has given an entire new life to photovoltaics research, in which basic considerations of efficiency, cost, freedom from toxicity, material availability in large quantities, and cell stability for long operating times have all become combined in a complex phenomenon involving the physical sciences, the social sciences, and political considerations. The Department of Energy has founded the Solar Energy Research Institute in Golden, Colorado, and photovoltaic research is a part of the charter of this institute. As a result the number of investigators and the interest in photovoltaics has increased by orders of magnitude over the past decade. As is common in such cases, there has also been an information explosion on photovoltaics, with a proliferation of books, whole journals, and literature, which makes comprehensive review an all but impossible task. The first major book heralding the new interest was Hovel's research treatise published in 1975 (*8*). Since then many other books and special journal issues have been added to the growing list of reviews of photovoltaics research (*9–24*).

Because of the magnitude of the task faced by a review in this area, this particular review is limited to solid state semiconductor junctions. Brief notice should be taken, however, of a variety of other photovoltaic effects of interest and/or significance. One of the oldest and most frequently explored effects is the so-called *anomalous photovoltaic effect* in which the measured open-circuit voltages often exceed the band gap of the material by an order of magnitude or more (*25–33*); the effect apparently arises from many junctions being present in the material, perhaps from crystallographic defects, adding in series. In the *thermophotovoltaic effect*, concentrated radiation is used to heat a metallic radiator which in turn illuminates a specially constructed photovoltaic cell (*34*); the goal is to make a better match between the spectral output of the radiator and the solar cell than exists between the solar spectrum and the solar cell, and to trap photons with energy less than the band gap of the solar cell material in order to help heat the radiator. An idealized model indicates a maximum theoretical efficiency of about 50% for a silicon solar cell and a radiator at 2200 K; efficiencies of 26% have been achieved to date experimentally. *Photoelectrochemical effects*, following Becquerel's initial discovery, are also being investigated; these involve the existence of a junction between a semiconductor and an electrolyte rather than a junction between or within semiconductors (*35*), and are related to the fundamental process that has produced many of our

traditional energy sources: photosynthesis. There are three major types of photoelectrochemical cells: (*a*) a photovoltaic cell, in which the chemical system is unchanged and only electrical power is extracted; (*b*) a photoelectrolysis cell, in which energy is extracted in the form of chemical redox reaction products (e.g., photoelectrolysis of water to produce H_2 and O_2); and (*c*) a photogalvanic cell (*36*), in which light absorption takes place in the electrolyte rather than in the semiconductor, and electrical power is subsequently generated by charge transfer to the electrode by a photooxidized or photoreduced molecule diffusing from the electrolyte.

II. An Overview of Photovoltaic Effects

In this section we give an overall survey of the types of semiconductor junctions involved in photovoltaic effects and the major processes and mechanisms that control junction currents and cell performance.

A. Types of Semiconductor Junctions

It is convenient to distinguish between four types of semiconductor junctions relevant to photovoltaic effects: (*a*) homojunctions, (*b*) heterojunctions, (*c*) buried or heteroface junctions, and (*d*) Schottky barriers.

1. *Homojunctions*

A homojunction is a junction formed between two portions of the same semiconductor material, one portion having n-type conductivity and the other p-type conductivity. A representative energy band diagram of a homojunction is given in Fig. 1, where the vacuum level has been included for reference. The electron affinity χ_s and the band gap E_G are the same on both sides of the junction. The diffusion voltage V_D, sometimes called the built-in voltage, results from the transfer of charge between n- and p-type portions required to maintain the Fermi level constant across the junction, and is given by the difference between the Fermi energies in the n- and p-type portions far removed from the junction. The drawing in Fig. 1 shows a symmetric distribution of the depletion region between n- and p-type portions, such as would be found if the carrier density in both n- and p-type portions were the same.

2. *Heterojunctions*

A typical band diagram for a heterojunction is given in Fig. 2. A heterojunction is a junction formed between two different semiconductor materials,

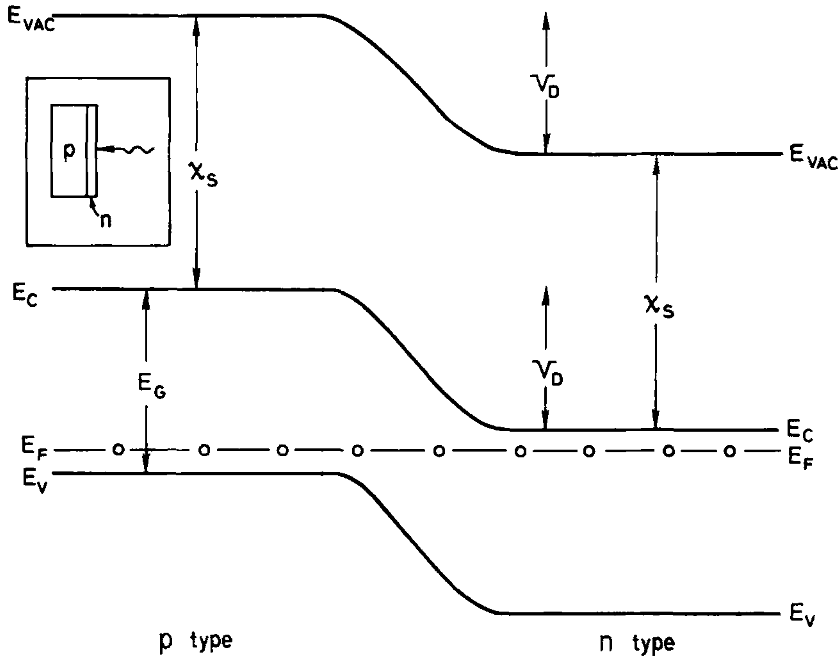

FIG. 1. Energy band diagram for a p–n homojunction in a semiconductor. Inset shows a typical geometry for a photovoltaic cell, with a narrow n-type region on a wider p-type region.

with different electron affinities and band gaps. One of the semiconductors is usually n-type and the other p-type. The diagram of Fig. 2 has once again been drawn with equal depletion layer widths on the two sides of the junction, for the specific case of equal carrier densities on both sides of the junction.

The construction of a band diagram for a heterojunction using only knowledge of bulk properties, such as electron affinity, band gap, and Fermi level position, is a hazardous exercise. Fairly complex processes can occur at the heterojunction interface resulting from interactions specific to the existence of the interface and not reflected in the bulk properties; for example, it is common for there to exist interface dipoles or interface states, the presence and charge of which may considerably change the band profiles at the interface. Figure 2 has been drawn in an idealized fashion following the Anderson abrupt junction model (*37*) in which interface states and dipoles have been neglected. This model calls for the band diagram to be drawn using only the bulk properties of the semiconductors, in such a way that discontinuities may occur in the conduction band and the valence band because of differences in electron affinity and band gap between the two semiconductors. Figure 2 has been drawn assuming values of these quantities

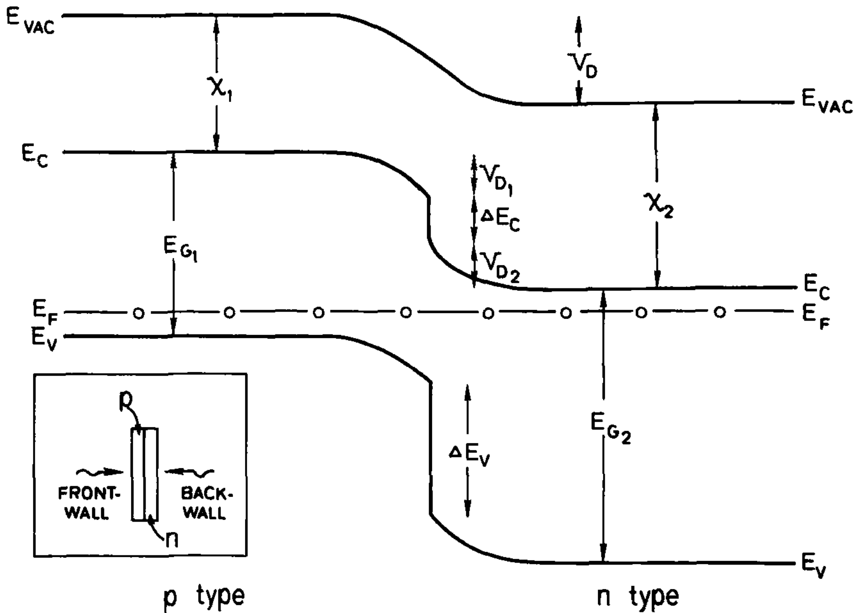

FIG. 2. Energy band diagram for a p–n heterojunction between two different semiconductors. Energy parameters of the two materials have been chosen so that no energy spike appears in either band. Inset shows two possible modes of operation as photovoltaic cells: (1) front-wall, with illumination incident on the p-type absorber, or (2) back-wall, with illumination incident on the n-type window.

such that these discontinuities do not contribute any "spikes" in the interface band structure. If χ_1 had been chosen to be larger than χ_2, on the other hand, the discontinuity in the conduction band would have resulted in an energy spike that would seriously impede electron transport from the p- to n-type portions. The p-type material has also been chosen to have the smaller band gap, a common situation since in general electron diffusion lengths in p-type material are larger than hole diffusion lengths in n-type material.

Deviations from an ideal heterojunction structure may arise from at least two other sources. Although it is possible to find two materials with the same lattice constant (e.g., GaAs has a lattice constant of 5.654 Å and Ge has a lattice constant of 5.658 Å), most heterojunctions consist of two materials with considerable lattice mismatch. Such lattice mismatch produces distortions and dislocations at the interface that give rise to localized interface states, which can play a large role in determining the photovoltaic properties of the junction. The second kind of deviation occurs because of the nature of real surfaces; when a junction is made by depositing one material on top of another, an intervening layer owing to the oxidized surface

of the second material or to chemical interaction or interdiffusion between the two materials may be formed. This intervening layer may control the properties of the junction. In certain cases a thin layer of insulating material, usually an oxide, is deliberately introduced to reduce the junction current; in this case, the junction is sometimes referred to as an SIS (semiconductor–insulator–semiconductor) structure. A basic principle guiding practical heterojunction research is that the properties of the junction may be determined not by the bulk properties of the individual materials, but by the process and interactions involved in junction formation.

3. *Buried or Heteroface Junctions*

Figure 3 shows a representative buried p–n junction formed by heterofacing with a p^+ material; such a junction consists of a heterojunction and a homojunction. The junction is called "buried" because it is the consequence of a narrow p-type region in the p^+–p–n junction illustrated in Fig. 3. The structure retains the advantage of a p–n homojunction and at the same time provides a different kind of front surface to the p-type material to minimize

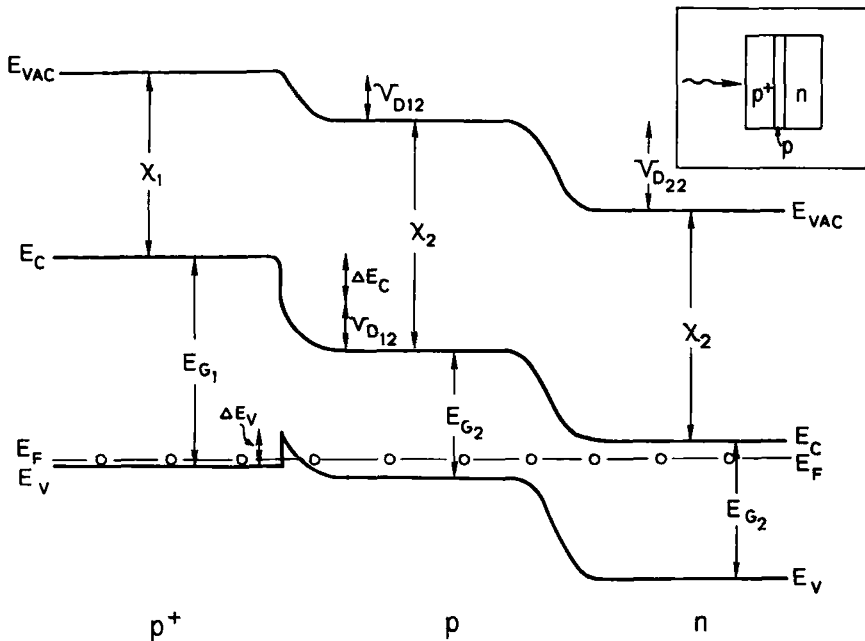

FIG. 3. Energy band diagram for a p^+–p–n heteroface buried junction in which the p^+ material acts as a large band-gap window and an ohmic contact to the p material. Inset shows the likely orientation of illumination for use as a photovoltaic cell.

surface losses. The narrow p-type region in the example of Fig. 3 may be formed before the addition of the p^+ heterofacing material, or in many cases it may be formed by diffusion fron the p^+ material in the process of junction formation. A heterofaced buried junction is usually preferable to a heterojunction of the two materials, since it moves the junction away from the heterojunction interface. The most efficient example of such a buried junction is the GaAlAs/GaAs cell (*38*), in which the p-GaAlAs is the heterofacing layer on a p–n GaAs junction; the lattice constant of AlAs is 5.661 Å and hence almost the same as that of GaAs, 5.654 Å, thus making possible a heteroface contact to the buried junction with minimized density of heteroface interface states.

4. *Schottky Barriers*

In many ways the Schottky barrier junction, consisting of the junction between a metal and a semiconductor, is the simplest of the junction types. A typical example is given in Fig. 4. It is also a simple model that neglects interface interactions and states and it predicts that a Schottky barrier is

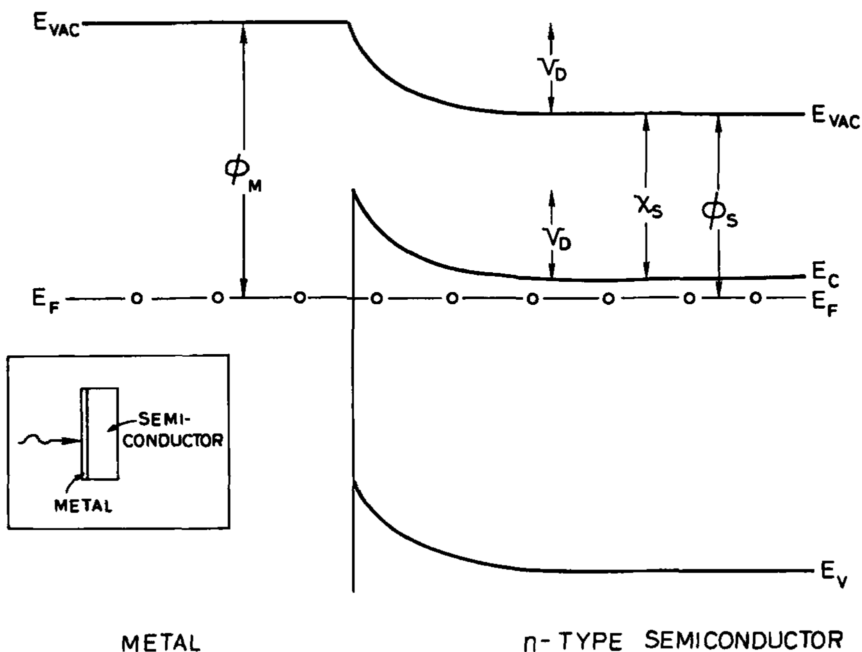

FIG. 4. Energy band diagram for a Schottky barrier on an n-type semiconductor, based on the simple energy parameters of the materials without inclusion of interface interaction effects. Inset shows the normal mode of operation as a photovoltaic cell.

formed on an n-type material if the work function of the metal ϕ_M is larger than the work function of the semiconductor ϕ_s. Such Schottky barriers are also sometimes prepared with an intervening insulator layer to minimize junction currents; such cells are called MIS (metal–insulator–semiconductor) junctions.

Research in recent years has shown that the simple argument advanced above for determining the barrier height of a metal–semiconductor junction does not hold for most materials of interest for photovoltaic cells (*39*). Evidence favors the conclusion that the location of the Fermi level at the surface of the semiconductor is controlled by interactions with the metal, less than a monolayer being sufficient (*40–44*). The actual height of a Schottky barrier must most often be determined experimentally.

B. Simple Photovoltaic Cell Model

A photovoltaic cell is evaluated in terms of its effectiveness in converting power from radiation into electrical power. A simple equivalent circuit is that of a current generator producing the light current $I_L = J_L A_L$, where A_L is the cell area exposed to illumination, which flows in the opposite direction to the forward current of a diode with diode current $I_D = J_D A_D$, where A_D is the total area of the junction.

$$I_D = I_0[\exp(\alpha V) - 1] \tag{1}$$

where I_0 is the reverse saturation current of the diode, and α is a parameter given by $\alpha = q/AkT$ with $A = 1$ for diffusion currents and $A \approx 2$ for recombination currents. For other junction current mechanisms that we discuss later, e.g., tunneling with or without thermal activation, the parameter α does not have the temperature dependence given above and may indeed be virtually temperature independent. In an ideal junction A_L may be taken equal to A_D, and expressions are commonly written in terms of current densities rather than currents; but in real cells this fundamental geometric difference between light and dark currents must be remembered. Figure 5 shows a typical equivalent circuit, including a series resistance R_s and a shunt resistance R_p.

In an ideal cell with no losses, the light current I_L is exactly that corresponding to one electronic charge crossing the junction and being collected in the external circuit for each photon incident on the cell with sufficient energy to be absorbed and create an electron–hole pair, i.e., usually a photon energy larger than the band gap. Since the quantum efficiency is defined as the number of electronic charges collected per incident photon, an ideal cell has a quantum efficiency of unity for photons with sufficient energy to create electron–hole pairs. The diode current I_D in such an ideal cell is no larger

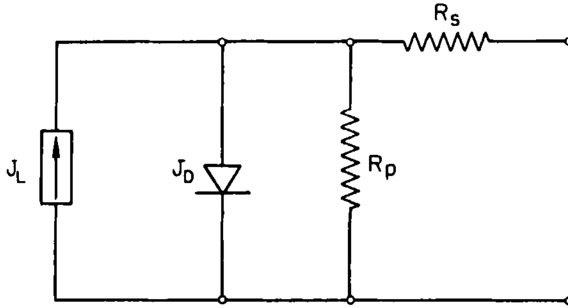

FIG. 5. Simple equivalent circuit for a photovoltaic cell, including a current generator, a diode, a series resistance, and a shunt or parallel resistance.

than the junction current associated either with diffusion of carriers over the junction barrier or with recombination of carriers near the junction. Other characteristics of an ideal cell are: (*a*) the parameters α and I_0 have the same values under illumination as in the dark; (*b*) the series resistance R_s is zero; and (*c*) the shunt resistance R_p is infinite.

Since the total current in such an ideal cell is obtained simply by superposing the light-generated and dark currents, the total current is given by

$$\begin{aligned} I &= I_D - I_L \\ &= I_0[\exp(\alpha V) - 1] - I_L \end{aligned} \tag{2}$$

The variation of I with V in the dark and under illumination corresponding to this model is shown in Fig. 6. The principle of superposition means that the dark I–V curve is simply lowered by the amount I_L to form the light I–V curve. This curve crosses the voltage axis ($I = 0$) at the open-circuit voltage V_{oc},

$$V_{oc} = \alpha^{-1} \ln[(I_L/I_0 + 1)] \tag{3}$$

and it crosses the current axis ($V = 0$) at the short-circuit current I_{sc},

$$I_{sc} = -I_L \tag{4}$$

These two simple results already reveal a basic key to the operation of a photovoltaic cell: The short-circuit current is controlled by the current generation and collection processes only, whereas the open-circuit voltage is controlled also by the magnitude of the diode current expressed through the parameters α and I_0. The forward current expressed through α and I_0 can be considered as a leakage path through which the buildup of the forward-bias voltage of the cell due to illumination can be dissipated; the

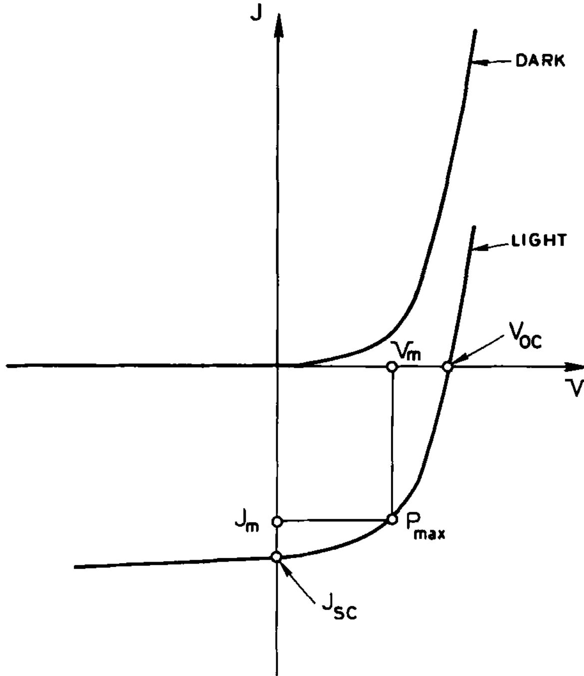

FIG. 6. Typical idealized light and dark J–V curves for a photovoltaic cell, showing the open-circuit voltage V_{oc}, the short-circuit current density J_{sc}, and the maximum power point P_{max}.

short-circuit current, on the other hand, is a current that flows in the reverse direction.

To evaluate the power generated by the cell, the shape of the light I–V curve is as significant as the magnitudes of V_{oc} and I_{sc}. At a particular point along the I–V curve, maximum power $P_m = I_m V_m$ is generated by the cell corresponding to a specific maximum power voltage V_m and maximum power current I_m. It is this maximum power that is used to calculate the efficiency of the cell η,

$$\eta = \frac{P_{max}}{P_{rad}} = \frac{I_m V_m}{P_{rad}} = \frac{I_{sc} V_{oc} \mathrm{ff}}{P_{rad}} \tag{5}$$

where P_{rad} is the total radiation power incident on the cell, and ff is called the fill factor and is a measure of the "squareness" of the I–V curve. From Eq. (5) the fill factor is defined as

$$\mathrm{ff} = I_m V_m / I_{sc} V_{oc} \tag{6}$$

The coordinates of the maximum power point can be determined by multiplying Eq. (2) by V and then maximizing the power with respect to V. For the ideal cell, the value of V_m is readily calculated by iteration from

$$V_m = V_{oc} - \alpha^{-1} \ln(\alpha V_m + 1) \tag{7}$$

The current for maximum power is then given by Eq. (2) with $V = V_m$.

An alternative method of calculating the fill factor of a cell is given by defining a parameter β,

$$\beta = (I_L + I_m)/I_L \tag{8}$$

This parameter corresponds to the current passing in the forward direction when the diode is biased at V_m in the dark, divided by I_L; by convention I_L is positive and I_m is negative. From the maximization of power calculation, an expression for β can be derived,

$$\beta = \left[1 + \ln\left(\beta \frac{I_L + I_0}{I_0}\right)\right]^{-1} \tag{9}$$

from which a value of β can be obtained by only a few iterations. For good cells β has a value between 0.04 and 0.10. In terms of β the fill factor can be expressed as

$$\text{ff} = \frac{(1 - \beta) \ln[\beta(I_L + I_0)/I_0]}{\ln[(I_L + I_0)/I_0]} \tag{10}$$

For an ideal cell the fill factor is not a function of the parameter α, but Eqs. (3) and (5) show that the efficiency is directly proportional to $1/\alpha$ through the dependence of V_{oc} on $1/\alpha$. A desired increase in efficiency cannot be achieved simply by increasing $1/\alpha$ (or A) because a complicated relationship between I_0 and α exists such that an increase in A usually corresponds to an increase in I_0 *(45)*.

C. More General Photovoltaic Cell Model

A somewhat more general model of a photovoltaic cell can be constructed by adding several nonideal features to the ideal model just discussed: a finite series resistance R_s and shunt resistance R_p, and allowance for the possibility that only a fraction of the light-generated carriers will actually be collected in the external circuit.

The presence of finite R_s and R_p results in power losses for the cell, which appear through reductions in the fill factor ff. An approximation to these effects can be made by assuming that the cell is operating near the maximum power point and that the loss can be described simply by $J_m^2 R_s$ for a series

resistance or V_m^2/R_p for a shunt resistance. The power loss fraction (PLF) for a series resistance is then

$$\text{PLF} = J_m^2 R_s / J_m V_m = J_m R_s / V_m \approx J_{sc} R_s / V_{oc} \tag{11}$$

which corresponds to PLF = 3% for $J_{sc} = 40$ mA/cm² and $V_{oc} = 0.6$ V if $R_s = 0.5\ \Omega$ per cm² of cell area. The power loss fraction for a shunt resistance is

$$\text{PLF} = (V_m^2/R_p)/J_m V_m = V_m / J_m R_p \approx V_{oc} / J_{sc} R_p \tag{12}$$

which corresponds to PLF = 3% for $R_p = 500\ \Omega$ per cm² of cell area. These simple calculations set the scale for the maximum tolerable value of R_s and the minimum tolerable value of R_p in an efficient cell. For small power losses, the decrease in cell efficiency is almost completely due to decrease in the fill factor, approximately by

$$\text{ff}(R_s, R_p) = \text{ff}(0, \infty)[1 - (J_{sc} R_s / V_{oc}) - (V_{oc} / J_{sc} R_p)] \tag{13}$$

Figure 7 shows a typical variation of ff with light-generated current and the effect of finite values of R_s and R_p on the fill factor. Measurement of this variation can prove a useful analytical aid in interpreting photovoltaic cell phenomena.

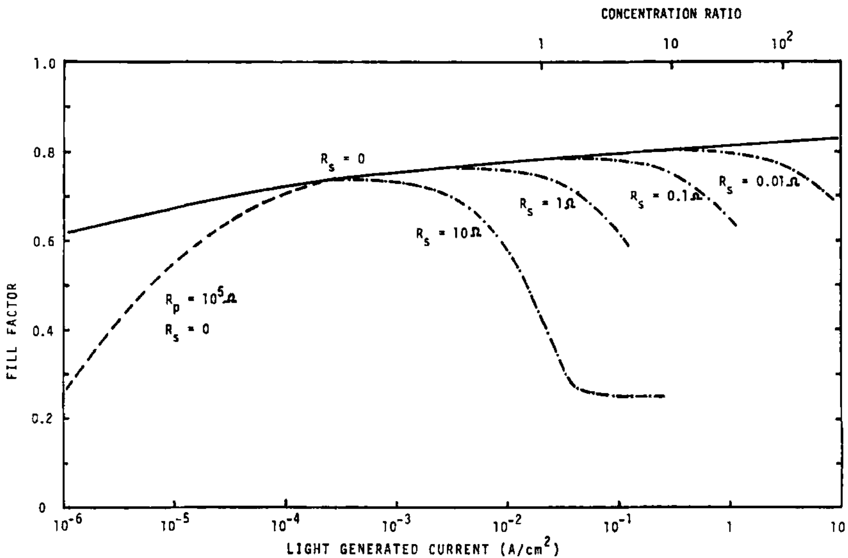

FIG. 7. Fill factor as a function of light current showing the effects of series and shunt resistance. The following parameters are assumed: $I_0 = 10^{-9}$ A/cm², $A = 1$, total active area = 1 cm², and an infinite shunt resistance R_p for all cases except the dashed curve, for which $R_p = 10^5\ \Omega$ and $R_s = 0$.

The $I-V$ relationship corresponding to Eq. (2) when R_s and R_p are included becomes

$$I = I_0\{\exp[\alpha(V - IR_s)] - 1\} + (V - IR_s)/R_p - I_L \tag{14}$$

The dynamic resistance $R_d = dV/dI$ is given by

$$R_d = \frac{1 + R_s(1 + R_s/R_p)^{-1} I_0\alpha \exp[\alpha(V - IR_s)]}{R_p^{-1} + (1 + R_s/R_p)^{-1} I_0\alpha \exp[\alpha(V - IR_s)]} \tag{15}$$

For sufficiently high forward voltages, when the second term in the numerator and denominator dominates, $R_d = R_s$. For small or negative voltages near or below the I_{sc} point on the curve, $R_d = R_p$. Thus both R_s and R_p can in principle be determined directly from the measured $I-V$ curve. The addition of a simple series resistance to the cell does not change V_{oc}, and decreases I_{sc} only when R_s is very large, in which case the $I-V$ curve approaches $1/R_s$ and the ff approaches its minimum value of 0.25. The addition of a simple shunt resistance to the cell does not change the value of I_{sc}, but may decrease the value of V_{oc} slightly.

The other nonideal factor mentioned earlier in this section is the presence of loss mechanisms for the photoexcited carriers to account for the possibility that some of the carriers may not be collected by the junction. A simple way to express this possibility formally is to introduce a collection function $H(V)$, which may also be a function of photon energy. By use of some simple collection functions, insight into the behavior of the cell can be obtained without requiring solution of nonequilibrium transport relations in the cell. Again this approach assumes that dark- and light-generated currents can be superposed, and so is reliable only within the constraints of that limitation. If such a collection function is introduced, Eq. (2) for the $I-V$ relationship becomes

$$I = I_0\{\exp[\alpha(V - IR_s)] - 1\} + (V - IR_s)/R_p - H(V)I_L \tag{16}$$

The function $H(V)$ is chosen to express the fraction of the photoexcited carriers that are actually collected. The general effects of a collection function with value less than unity, having a smaller value the higher the forward bias, is again primarily to reduce the fill factor, with only minor reductions in V_{oc} and I_{sc} in efficient cells.

Let us consider as an example of the application of this collection function approach the case of a p–n heterojunction where the n-type material is the large band gap material which can be ignored in the photogeneration process, and where the depletion layer is almost totally in the p-type material, since n is larger than p. We make the following reasonable construction of the collection function. We divide the collection function $H(V)$ into two portions

so that $H(V) = g(V)h(V)$, where $g(V)$ describes the loss of carriers to recombination in the bulk of the p-type material beyond the depletion region (those carriers created far from the junction having a higher probability of recombining before diffusing to the junction than carriers generated nearer the junction), and where $h(V)$ describes the loss of carriers to recombination at the junction interface due to interface states. Both $g(V)$ and $h(V)$ may be functions of wavelength as well, but it is expected that $g(V)$ will vary strongly with wavelength because of the variation of absorption constant with wavelength, and that $h(V)$ will be relatively wavelength independent. The collection function $g(V)$ can then be calculated as follows (*46, 47*):

$$g(V) = \frac{\int_0^W \exp(-ax)\,dx + \int_W^\infty \exp(-ax)\exp[-(x - W)/L_n]\,dx}{\int_0^\infty \exp(-ax)\,dx} \tag{17}$$

The wavelength dependence enters through the variation of the absorption constant $a(\lambda)$. The first term in the numerator of Eq. (17) describes the collection of carriers generated within the depletion layer of width W, under the assumption that all carriers generated within W are collected because of the assisting drift field there. The second term in the numerator of Eq. (17) expresses the loss of carriers generated beyond W if the diffusion length of electrons in the p-type material is L_n. Integration of Eq. (17) yields

$$g(V) = 1 - \frac{\exp(-aW)}{1 + aL_n} \tag{18}$$

The voltage dependence enters through the voltage dependence of the depletion layer width W,

$$W(V) = (2\epsilon/qN_A)^{1/2}(V_D - V)^{1/2} \tag{19}$$

One approach of obtaining an expression for the interface collection function $h(V)$ is to make use of the approximate collection function proposed by Rothwarf (*48*). Assuming that recombination at the interface can be described by an interface recombination velocity s_I, and that the recombination probability could be viewed as a simple competition between crossing the junction without recombination and recombining at the interface, the following interface recombination function is useful:

$$h(V) = (1 + s_I/\mu\mathscr{E})^{-1} \tag{20}$$

where μ is the mobility of carriers at the interface, and $\mathscr{E}$ is the electric field at the interface given by $\mathscr{E} = 2(V_D - V)/W(V)$. If there are N_I interface states per cm^2 at the interface with a capture coefficient of B cm^3/sec, then $s_I = N_I B$.

Figure 8 shows the spectral response of quantum efficiency for a CdS/CdTe heterojunction cell, which seems to meet the requirements assumed above for the particular collection functions derived (*47*). The cell was made by vacuum evaporation of a high-conductivity n-type CdS film onto a p-type single crystal of CdTe. The high and low energy cutoffs of the spectral response curve of Fig. 8 correspond to the band gaps of CdS and CdTe, respectively. Between these two cutoffs, a wavelength-dependent effect is seen in which the quantum efficiency increases with decreasing wavelength, corresponding to increasing absorption constant a, which can be described by the $g(V)$ function with almost negligible dependence on V over the experimental range shown. Also seen is a wavelength-independent effect in which the quantum efficiency at all wavelengths increases with reverse bias, which can be described by the $h(V)$ function with a value of 0.84 at zero bias and 0.89 at a bias of -1 V. Consistent description with all cell parameters is obtained if $s_I = 2 \times 10^6$ cm/sec, which is reasonable for this heterojunction in which the two members show a large lattice mismatch of about 9%.

Inclusion of the collection function $H(V)$ in Eq. (16) means that expres-

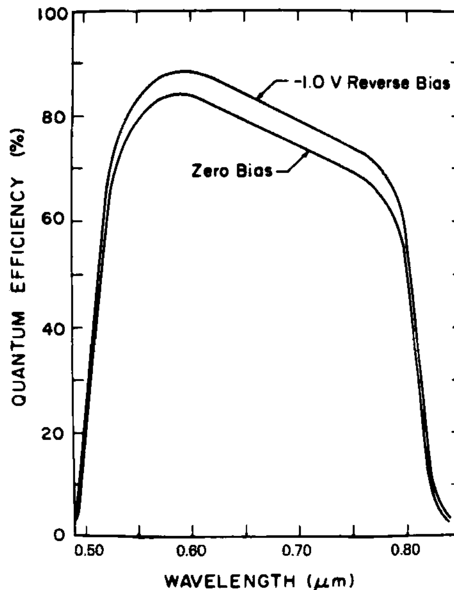

FIG. 8. Spectral dependence of the quantum efficiency for a CdS/CdTe heterojunction cell prepared by vacuum evaporation of CdS on single crystal CdTe. [From Mitchell *et al.* (*47*).]

sions for photovoltaic parameters are altered. The open-circuit voltage becomes

$$V_{oc} = \alpha^{-1} \ln\left[H(V_{oc})\frac{I_L}{I_0} + 1 - \frac{V_{oc}}{I_0 R_p}\right] \tag{21}$$

and the short-circuit current becomes

$$I_{sc} = (1 + R_s/R_p)^{-1}[I_0 \exp(-\alpha I_{sc} R_s) - I_0 - H(0) I_L] \tag{22}$$

The dynamic resistance has an additional term added to the denominator of Eq. (15) consisting of $-I_L\, \partial H(V)/\partial V$, so that for small or negative values of voltage near I_{sc},

$$R_d = [R_p^{-1} - I_L\, \partial H(V)/\partial V]^{-1} \tag{23}$$

The observation of a finite slope of the $I-V$ curve through the short-circuit point may be caused, therefore, either by a shunt resistance or by a voltage-dependent collection function.

Another departure from ideality occurs if the junction parameters vary with illumination. For an ideal cell, elimination of I_L between Eqs. (3) and (4) shows that the relationship between I_{sc} and V_{oc} is identical to that between I and V from Eq. (2). The variation of I_{sc} with V_{oc} as the illumination intensity is varied is often measured as a test of the independence of the junction parameters on illumination. If the $I_{sc}-V_{oc}$ is identical with the $I-V$ dark curve, it is concluded that the junction transport is not affected by light. In the more general case, however, in which R_s, R_p, and $H(V)$ effects need to be considered, coincidence between $I_{sc}-V_{oc}$ and dark $I-V$ curves is obtained only if the junction parameters α and I_o, R_s, and R_p are independent of illumination, if R_s is sufficiently small, and if $H(0) = H(V_{oc})$, as can be seen by eliminating I_L between Eqs. (21) and (22), and comparing with Eq. (16).

D. Major Processes and Mechanisms

A representative diagram of a junction, applicable to any of the junctions described in Section II,A with suitable modifications, is given in Fig. 9. For the sake of the specific discussion that follows, we will consider light being incident on the n-type face of the junction in Fig. 9, this n-type region representing the conditions at the front surface of a homojunction, the front surface of a heterojunction, the n-type region of a buried n–p junction, or the metallic layer of a Schottky barrier. In this section we trace in a qualitative manner the phenomena involved in current generation, current collection, and junction transport.

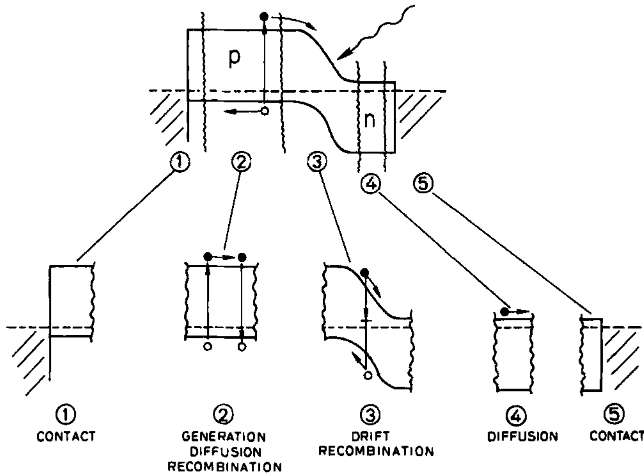

FIG. 9. Breakdown of the processes taking place in a representative photovoltaic junction. It is assumed that the light is incident on the n-type end.

1. *Reflection*

The first consideration in determining current generation by the light is the proportion of light lost immediately due to reflection from the front surface of the semiconductor. The refractive index of most semiconductors is relatively large, corresponding to reflectivities of 20–40%. Such reflection losses can fortunately be minimized by using a large-band-gap, electrically inert, interference layer, designed in a simple case so that its thickness is a quarter-wavelength within the semiconductor of the radiation wavelength at the maximum of the solar spectrum. Use of a single such layer can reduce the reflectivity most effectively only at one wavelength, of course, but often the improvement achievable is sufficient. Greater reduction in reflection over a wider wavelength range can be achieved by using multiple antireflection layers.

2. *Contact Area*

If opaque contacts cover a fraction of the illuminated surface of the junction, the illuminated area A_L useful in current generation is less than the junction area A_D active in producing the junction current, as mentioned in Section II,B. Considerable engineering ingenuity is devoted to the task of minimizing the contact area while retaining good current collection by these contacts. One solution that shows promise is to use a high-conductivity degenerate large-band-gap transparent layer (like In_2O_3, SnO_2, $CdSnO_4$,

or ZnO) for the contact so that only a minimal area must be obscured by opaque contact to this transparent conducting layer.

3. *Contact Resistance*

One of the major contributions to the series resistance R_s of the cell sometimes comes from the resistance of the contacts, particularly in novel or experimental cells made with materials not technologically developed. The desirable choice, of course, is to have an ideal ohmic contact that provides the minimum resistance achievable. If metal–semiconductor interaction effects do not dominate, an ohmic contact is provided by a metal with work function less than the work function of an n-type semiconductor, or greater than the work function of a p-type semiconductor. It is usually found beneficial in addition to have a mild heat treatment to diffuse in the metal, which has been chosen to be an n-type impurity (p-type impurity) in an n-type (p-type) semiconductor; this diffusion increases the carrier density in the semiconductor at the contact interface and reduces the contact resistance, which is relatively strongly dependent on the carrier density at the semiconductor surface. As an example, the ohmic (linear I–V curves in all cases) contact resistance of In contacts on InP crystals has been measured for electron densities in the n-type InP between 5×10^{17} and 5×10^{15} cm^{-3}; over this range the contact resistance varies from 10^{-2} to $10\ \Omega \cdot \text{cm}^2$ (*49*). Any contribution to the total series resistance becomes critical if concentration of sunlight is used, and the total series resistance in AlGaAs/GaAs solar cells, for example, must be of the order of $10^{-4}\ \Omega \cdot \text{cm}^2$ or less for concentrations of the order of 10^3. Our estimate in Section II,C of $0.5\ \Omega \cdot \text{cm}^2$ for the maximum allowed series resistance for the entire cell indicates that the contribution to R_s from any single contact must be much less than this.

For some materials of promise for solar cells, e.g., p-type cadmium telluride, no metal exists with an appropriate work function to form an ideal ohmic contact. Another alternative remains in such cases. If the surface of the semiconductor can be made sufficiently conducting, the depletion layer formed by the Schottky barrier of the nonohmic contact in the semiconductor is thin enough to allow tunneling through it. Such a contact may be relatively low resistance and ohmic at one temperature, but may become rectifying and high resistance if the device is cooled appreciably, particularly if the dominant tunneling process is thermally assisted.

4. *Collection Resistance*

As we continue toward the left in the diagram of Fig. 9, we encounter next the problem of collection resistance. This is to first order simply the

resistance of the n-type region through which the current must travel to be collected. If the complete area of the semiconductor can be covered with the contact, as with a transparent high-conductivity layer for this n-type region, then the resistance corresponds to the thickness of the semiconductor material; if a contact grid is used, then the resistance involves the lateral flow of current to the grid as well as the flow of current normal to the junction through the semiconductor. If the n-type layer we are considering is a polycrystalline layer rather than a single crystal layer, then the lateral current flow can be impeded still further by the presence of intergrain potential barriers in the layer which reduce the effective carrier mobility $\mu = \mu_0 \exp(-E_b/kT)$, where E_b is the height of the intergrain barriers (*50*).

In practical cells, design of the grid structure to minimize the collection resistance has been advanced to a fine art (*51*) and has been approached analytically using various lumped element equivalent circuits (*52–55*) and finite element models (*56*).

There is, of course, also a contribution to the collection resistance from the p-type material in Fig. 9, just as there is a contribution from the back contact resistance to the p-type material. Since the n-type region is usually much thinner than the p-type region, however, the resistivity of the n-type layer must usually be several orders of magnitude smaller than that of the p-type region (of the order of tenths or hundredths of an $\Omega \cdot$cm compared to tens or hundreds of $\Omega \cdot$cm, respectively).

5. *Optical Absorption*

In order to create electron–hole pairs the incident light must be absorbed by the semiconductor. For a homojunction there will be contributions to the total current from absorption in both the n-type and p-type regions. For a heterojunction in which the n-type region is a high band gap material, useful absorption may take place primarily in the p-type material. For a Schottky barrier absorption takes place in the p-type material of Fig. 9 after being transmitted through the metallic layer (replacing the n-type layer in Fig. 9), which must be kept very thin therefore to allow maximum transmission to the semiconductor.

The major contribution to the optical absorption comes from transitions across the band gap of the semiconductor, caused by photons with energy equal to or greater than this band gap. If the band gap transition is an optical direct transition, i.e., if the extrema of the conduction band and valence band occur at the same value of **k**, the absorption constant increases very rapidly with photon energy at the band gap energy and quickly reaches values in the 10^4–10^5 cm^{-1} range. The penetration depth of the light (equal to the reciprocal of the absorption constant) is therefore about a few tenths of a

micrometer for a direct-band-gap material, and the required thickness of the material to absorb all the light is only two or three times the penetration depth. If the band gap transition, on the other hand, is an optical indirect transition, i.e., the extrema of conduction and valence bands occur at different values of **k**, the absorption constant increases more gradually for photon energies greater than the band gap, and thicknesses of about a hundred micrometers are required to absorb all of the light. Among materials used for solar cells, only silicon has an indirect band gap; others such as GaAs, InP, CdTe, etc. all have direct band gaps. If thin-film cells are desired with a total thickness of not more than about 10 μm, only direct-band-gap materials can be used.

If a photon flux $F_0(\lambda)$ is incident at $x = 0$ on the absorbing material, the photon flux $F(\lambda, x)$ at a distance x inside the material is given by

$$F(\lambda, x) = F_0(\lambda) \exp[-a(\lambda)x] \tag{24}$$

where $a(\lambda)$ is the absorption constant of the light. Usually the flux F is measured either in mW/cm^2 or $photons/cm^2$ sec. Sunlight falls on the earth with a flux of about 100 mW/cm^2. The rate of carrier generation because of the absorption of this radiation is given by

$$G(\lambda, x)\, dx = -dF(\lambda, x) = a(\lambda)F(\lambda, x)\, dx \tag{25}$$

This was the kind of expression used in the calculation of Eq. (17).

Two considerations compete with each other. In order to achieve absorption of the largest portion of the solar spectrum, as given in Fig. 10, it is

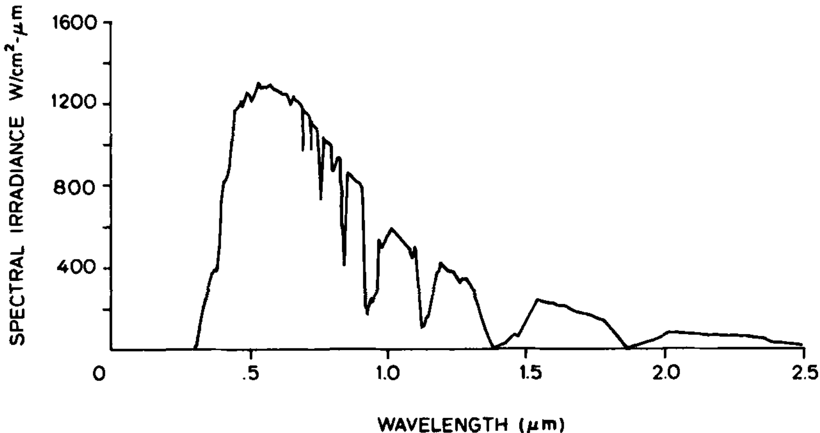

FIG. 10. Standard AM1.5 solar spectrum, computer generated from data measured in space. [From *Terrestrial Photovoltaic Measurement Procedures*, ERDA/NASA/1022-77/16, NASA TM 73702, NASA-Lewis Research Center, Cleveland, Ohio 44135 (1977).]

desirable to have as small a band gap as possible so that every photon in the solar spectrum has enough energy to create an electron–hole pair. However as the band gap decreases, the magnitude of J_0 inevitably increases (see Section IV). These competing considerations lead to the conclusion that there is an optimum band gap that will allow the best absorption with the smallest J_0. A classic calculation of this type for ideal homojunctions with no surface recombination losses by Loferski (*57*) indicates that an optimum band gap occurs at about 1.4 eV for recombination-controlled junction currents and at about 1.6 eV for diffusion-controlled currents. The maximum, however, is broad and suggests that specific circumstances might warrant use of any semiconductor with a band gap in the range between 1.0 and 2.0 eV. Loferski's results are shown in Fig. 11.

Because of these considerations the choice of a specific band gap semiconductor means that all photons with energy less than this band gap do not create electron–hole pairs and therefore contribute to an overall loss of efficiency. The absorption of photons with much larger energy than the band gap also contribute to a loss, since the extra energy of the photons is simply dissipated as phonons as the excited carriers return to thermal equilibrium

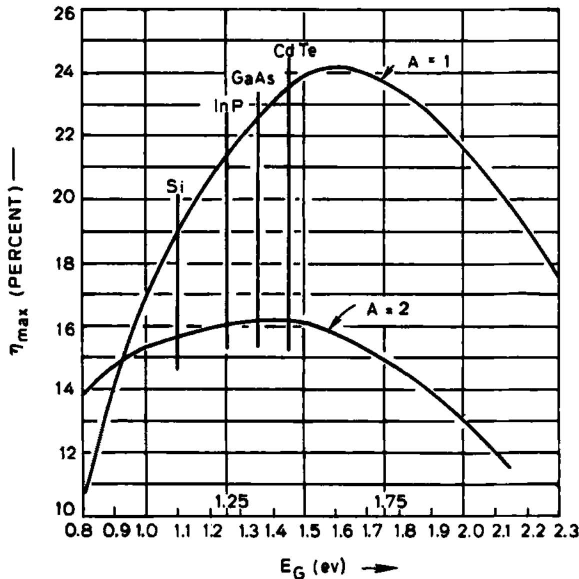

FIG. 11. Theoretical solar efficiency vs. semiconductor bandgap for ideal homojunction photovoltaic cells with no surface recombination loss. Curves are calculated for junction current due to injection ($A = 1$) and to recombination in the depletion layer ($A = 2$). [From Loferski (*57*).]

in the band; it is toward a reduction of this loss that the thermophotovoltaic device described in Section I is directed. If a heterojunction is used, then the number of available photons is reduced still further; for the CdS/CdTe heterojunction with spectral response shown in Fig. 8, only 44% of the solar spectrum is contained in the "window" between the band gaps of CdS and CdTe.

6. *Carrier Collection*

If Fig. 9 represents a homojunction, then electrons generated by photoabsorption in the p-type material that are able to cross the junction by diffusion and be collected, and holes generated by photoabsorption in the n-type material that are able to cross the junction and be collected, constitute the current. If Fig. 9 represents a heterojunction or a Schottky barrier, then primarily electrons created in the p-type region that cross the junction and are collected constitute the current. Since carriers must be created within about a diffusion length $L_n = (\mu\tau_n/kT)^{1/2}$ of the junction (where τ_n is the electron lifetime in the p-type material) in order to be collected before recombination occurs, only those carriers created within a diffusion length of the junction contribute to the current. This means than an indirect-band-gap material must have much larger values of diffusion length for the minority carriers than a corresponding direct-band-gap material, since optical generation of carriers is spread out over a much larger distance in the indirect-band-gap material.

Carrier collection can be aided by the presence of electric fields, Carriers generated in the depletion layer, for example, are almost all collected without loss, because of the local field as well as the proximity to the junction. In principle a built-in electric field might be developed across the whole absorbing region of the semiconductor by suitable choice of a gradient of impurity density, but in practice this has not been used for most materials because it is difficult to produce the desired impurity gradient without causing a decrease in minority carrier lifetime, and because such a built-in field automatically reduces the value of V_{oc} that can be obtained owing to its reduction of the diffusion potential of the junction. The existence of such a drift field would probably be essential for the successful operation of low-lifetime materials *(58)*.

7. *Surface Recombination*

If Fig. 9 represents a homojunction, then carriers generated by light in the n-type region may also diffuse to the surface as well as toward the junction to be collected. Because the surface of most materials consists of a relatively high defect density, the probability for recombination is usually

larger at the surface than in the bulk. Carriers that diffuse to the surface, therefore, are lost through recombination. Particularly if the material has a direct band gap, the illuminated n-type portion of the junction must be very thin to allow light to penetrate to the junction, but this means that a high density of carriers is generated close to the front surface where they can be lost through surface recombination. For this reason the quantum efficiency of a homojunction usually decreases with increasing photon energy, as the increasing absorption constant associated with the higher photon energies causes carrier creation to occur nearer to the front surface of the n-type material.

Losses due to surface recombination can be reduced by incorporation of an electric field at the surface that produces a potential barrier for minority carriers moving toward the surface by suitable impurity doping, by surface passivation in which a specific recipe is developed by which the surface recombination states may be rendered less effective, or by the use of a buried homojunction structure with a suitable heteroface junction at the front surface of the homojunction so that surface states (now interface states) are reduced. In the AlGaAs/GaAs heteroface buried homojunction cell, the front surface of the GaAs p–n junction is converted from a free surface to an AlGaAs/GaAs interface with good lattice matching and few interface states, whereas the free surface of the AlGaAs is not important in the current generation process.

8. *Interface Recombination*

We have already introduced the concept of interface recombination in Section II,C, where the effect was described in terms of the interface recombination velocity of the collection function $h(V)$. If Fig. 9 represents a heterojunction, then the interface between the two different p- and n-type materials is likely to consist of additional localized states that play a role in recombination similar to the one the surface states have on the front surface of the homojunction. Electrons generated in the p-type material may recombine via these interface states and fail to be collected by the junction. Since these states lie in a region of high electric field at the junction, they need not have a major deleterious effect on current collection; indeed, quantum efficiencies close to unity have been achieved in heterojunctions like ZnO/CdTe for which the lattice mismatch is close to 30% (*59*). On the other hand, such interface states provide a transport path for forward currents and thus lead to a reduction in V_{oc}.

9. *Grain Boundaries in Polycrystalline Films*

If one or both members of the photovoltaic junction have the form of polycrystalline films rather than single crystals, additional effects may be attributed to the grain boundaries in the polycrystalline films. If the grain

size is smaller than the diffusion length of the carriers, there may be appreciable loss of photoexcited carriers by recombination at grain boundaries, thus causing a decrease in the short-circuit current. If the grain boundaries intersect the junction, there may be additional paths for current transport, thus reducing the open-circuit voltage. In Section II,D,4 we have already mentioned the effect of such polycrystalline films on increasing the collection resistance.

An example of the effect of polycrystalline vs. single crystal cell behavior is given by the investigation of CdS/InP junctions prepared on both single crystal (*60–62*) and polycrystalline InP (*60*, *63*). In this case it was possible to obtain almost the same short-circuit current with the polycrystalline InP as with the single crystal InP, but the open-circuit voltage was appreciably reduced by grain-boundary induced leakage currents. Figure 12 compares CdS/InP cell properties (each type of cell was made by chemical vapor deposition of thin-film CdS onto the InP substrate) for the two types of cell; the junction current is about 100 times larger for the cell made with polycrystalline InP, corresponding to a reduction in V_{oc} from 0.79 V in the single crystal cell to 0.46 V in the polycrystalline cell.

10. *Back Contact*

In Section II,D,4 we mentioned the contributions of the collection resistance of the p-type material in Fig. 9, and of the back contact to this p-type material. Since this back contact does not have to be designed to allow light

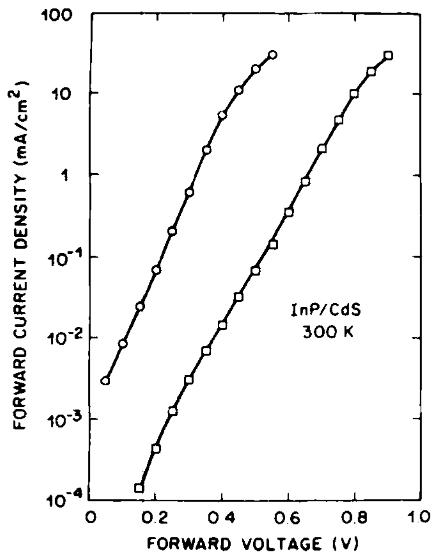

FIG. 12. Forward bias current–voltage curves for CdS/InP heterojunctions for single-crystal (□—□) InP and for polycrystalline thin film (O—O) InP. [From Shay *et al.* (*60*).]

transmission, a large area contact can be used to minimize contact resistance. In cells in which the p-type region thickness is comparable to the diffusion length of photoexcited minority carriers, there may be some loss of carriers due to recombination at the back surface, like the front surface recombination loss described in Section II,D,7. A short diffusion of additional dopant at the back surface can minimize this loss by providing a surface electric field that impedes the flow of carriers to the surface (*64*); an increase in hole density in the p-type material near the back surface, for example, produces a barrier for minority-carrier electron diffusion to that surface.

11. *Junction Current Mechanisms*

The final topic in this survey of photovoltaic processes is the origin of the junction current itself, that forward-biased current that reduces the ability of the junction to sustain a forward voltage and hence reduces the open-circuit voltage. The simplified model of Fig. 13 illustrates the principal

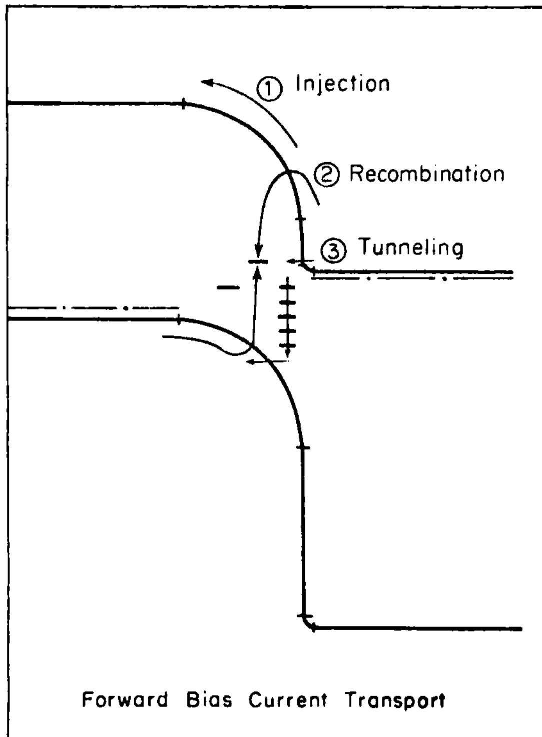

FIG. 13. Simple indication of three major modes of forward junction current: (1) injection over the barrier, (2) recombination in the depletion layer, and (3) tunneling, with or without thermal assistance, through interface or imperfection states, followed by recombination.

transport mechanisms, which we describe in somewhat more detail in Section IV.

The most ideal behavior and that corresponding to the smallest value of junction current occurs when the junction current is controlled by diffusion over the barrier, which is associated with the injection of electrons from the n-type material to the p-type material in Fig. 13. This ideal behavior corresponds to $A = 1$ in Eqs. (2) and (16).

The second most desirable ideal behavior, corresponding to the next smallest value of junction current, is associated with current transport through the junction by recombination in imperfection states in the depletion region. If these states lie at midgap, then the factor $A \sim 2$, although it may actually take on values between 1 and 2 in real situations.

Additional junction current may result if interface states are present, since it is then possible for junction current to flow via recombination in the interface states.

Usually the largest junction currents are the result of tunneling from the n-type material in Fig. 13 either to interface states or to imperfection levels, with subsequent recombination with holes in the p-type material. Such tunneling may occur without thermal activation if the interface barrier is thin enough, or more generally it occurs with thermal activation increasing the electron energy such that tunneling becomes highly probable. When tunneling dominates the junction current the parameter α is no longer given by q/AkT, but α varies more slowly with temperature and may indeed be temperature independent altogether. In many real situations in which the measured current–voltage curves of a junction indicate tunneling-dominated transport, the expected depletion layer width at the junction calculated from the known bulk carrier density is simply too wide to allow tunneling (*59*, *65*); this behavior must then be interpreted as a high density of charge residing near the interface in bulk imperfections or interface states, which reduces the depletion layer width sufficiently to allow tunneling.

III. Current Generation

In Sections III and IV of this review we consider in more detail the specific processes of current generation and junction currents, since these are the two principal contributors to the short-circuit current and the open-circuit voltage, respectively.

Current generation is commonly described in terms of what is known as the transport equation for photoexcited carriers. The transport equation correlates carrier generation with recombination, diffusion, and drift of the photoexcited carriers. If the transport equation can be solved with the appropriate boundary conditions, we are able to express the light-generated

current of the photovoltaic cell. Section II,C has described some of the attempts to circumvent general solution of the transport equation by the use of partially ad hoc collection functions. Even in this more detailed discussion we focus on specific cases of solution of the transport equation, since general solutions are usually so complex as to obscure physical significance.

Simple solutions of the transport equation are possible in the case where the dark and light currents of the junction can simply be superposed as in Eq. (2) (*66–68*). This superposition is valid when the differential equations and the boundary conditions of the system are linear with respect to the carrier densities and their derivatives; it is this linearity that makes it possible to sum directly dark and light currents. The discussion given here is in the form suitable to a p-type absorbing material, for reasons discussed earlier, and is with slight modification equally applicable to either a homojunction, a heterojunction, or a Schottky barrier, since the active region being considered is in the p-type material.

A. Derivation of the Transport Equation

Under illumination the time rate of change of minority carriers in the p-type material is described by

$$dn_p/dt = G(x) - U(x)$$
$$= a(\lambda)F - (n_p - n_{p0})/\tau_n \tag{26}$$

where $G(x)$ is the generation rate given by Eq. (25), and $U(x)$ is the recombination rate expressible in terms of the thermal equilibrium minority carrier density n_{p0} and the lifetime of minority carriers τ_n.

The current density is given by the sum of drift and diffusion components for both electrons and holes:

$$\mathbf{J}_n = nq\mu_n\mathscr{E} + qD_n\,\nabla n \tag{27}$$

$$\mathbf{J}_p = pq\mu_p\mathscr{E} - qD_p\,\nabla p \tag{28}$$

where μ_n and μ_p are the mobilities of electrons and holes, respectively; and D_n and D_p are the diffusion coefficients for electrons and holes, respectively. The corresponding continuity equations are

$$\partial n/\partial t - \nabla\cdot\mathbf{J}_n/q = G_n - U_n \tag{29}$$

$$\partial p/\partial t + \nabla\cdot\mathbf{J}_p/q = G_p - U_p \tag{30}$$

Since electrons and holes are generated in equal densities by optical transitions across the band gap of the material, $G_n = G_p$ and $U_n = U_p$. Here we

neglect departures from charge neutrality, which may occur in transient cases for strong gradients in the generation rate, and carrier trapping effects. Combination of Eqs. (27)–(30) yields the set of one-dimensional transport equations for n and p:

$$\frac{\partial n}{\partial t} = D_n \frac{\partial^2 n}{\partial x^2} + \mu_n \mathscr{E} \frac{\partial n}{\partial x} + \mu_n n \frac{\partial \mathscr{E}}{\partial x} - \frac{n - n_0}{\tau_n} + G_n(x) \tag{31}$$

$$\frac{\partial p}{\partial t} = D_p \frac{\partial^2 p}{\partial x^2} - \mu_p \mathscr{E} \frac{\partial p}{\partial x} - \mu_p p \frac{\partial \mathscr{E}}{\partial x} - \frac{p - p_0}{\tau_p} + G_p(x) \tag{32}$$

A totally general solution requires that these two equations be solved simultaneously with Poisson's equation. Under the condition, however, that $G_n = G_p$, $p \gg n$ (for our case, or alternatively $n \gg p$ for an n-type absorber), and steady state holds ($\partial n/\partial t = \partial p/\partial t = 0$), Eqs. (31) and (32) can be uncoupled and a single equation written for the minority carriers n_p in the p-type material being described here (*66, 69, 70*).

$$D_n \frac{d^2 n_p}{dx^2} + \mu_n \mathscr{E} \frac{dn_p}{dx} - \frac{n_p - n_{p0}}{\tau_n} + G(x) = 0 \tag{33}$$

This approximation breaks down if the minority carrier density excited by light becomes comparable to the majority carrier density, as is the case, for example, under very high light intensities or at high forward bias (*71, 72*).

B. *Solution of the Transport Equation*

1. *Boundary Conditions*

A common assumption is that at the edge of the depletion layer in the p-type material the density of minority carriers is equal to the density in thermal equilibrium for zero applied bias, since excess minority carriers will be swept out rapidly by the junction field. Then for a forward-bias voltage V, the carrier density at the edge of the depletion layer in the p-type material is given by

$$n_p = n_{p0} \exp(qV/kT) \tag{34}$$

2. *A Semi-Infinite Absorber*

If the absorbing material is sufficiently thick that penetration of light to the back of the material can be neglected (i.e., the thickness is much larger than either the penetration depth of the light or the diffusion length of the minority carriers), a relatively simple solution of Eq. (33) can be obtained. It is further commonly assumed that the electric field in the neutral region

of the p-type material away from the depletion layer is zero. Equation (33) becomes

$$\frac{d^2n_p}{dx^2} - \frac{n_p - n_{p0}}{D_n\tau_n} = -\frac{G(x)}{D_n} = -\frac{a(\lambda)F}{D_n}\exp(-ax) \tag{35}$$

where x is measured positively into the p-type material with origin at the edge of the depletion layer, and F is the light intensity at the edge of the depletion layer. The boundary conditions are given by Eq. (34) at the edge of the depletion layer, and by n_p going to n_{p0} as x goes to infinity. Equation (35) can be solved for n_p, and then the diffusion electron current $J_n(x)$ is given by $qD_n(dn_p/dx)$. The result for the electron current is (*24*)

$$J_n(x) = -\frac{qD_n n_{p0}}{L_n}\exp\left(\frac{-x}{L_n}\right)\left[\exp\left(\frac{qV}{kT}\right) - 1\right] + \frac{qa(\lambda)F(\lambda)}{a^2 - 1/L_n^2}\left[a\exp(-ax) - \left(\frac{1}{L_n}\right)\exp\left(\frac{-x}{L_n}\right)\right] \tag{36}$$

The first term represents the dark current density due to diffusion of minority carrier electrons; it is not affected by illumination. Similarly the second term represents the light current density and is not affected by applied voltage. Because of the linearity of the equations in n_p, the principle of superposition holds, and dark and light currents simply add; this would not be true, for example, if the lifetime τ_n were a function of n_p, or if generation and recombination in the depletion layer depend on J_n (*73–75*). At the depletion layer edge $x = 0$, and with $V = 0$, Eq. (36) yields

$$J_n(0) = \frac{qF(\lambda)}{1 + 1/a(\lambda)L_n} = J_L(\lambda) \tag{37}$$

for the monochromatic light of wavelength λ.

3. *A Finite Absorber with Back Surface Recombination*

If we need to consider a finite absorber with a surface recombination velocity s at the back surface, we need to add the additional boundary condition that

$$J_n = (n_p - n_{p0})qs = -qD_n\, dn_p/dx \tag{38}$$

at the back surface. The presence of a back surface field as discussed in Section II,D,10 would clearly require modifications in the transport equation. Solutions involving the boundary condition given by Eq. (38) show the expected decrease in electron density near the back surface for appreciable magnitudes of s there (*8, 24*).

C. Other Contributions to Current Generation

Finite contributions to current generation may also be expected in a total p–n junction from the depletion layer and the n-type material as well as the p-type material described earlier. Since all the carriers generated in the depletion layer may be assumed to be collected because of the high junction field, the contribution to the current from absorption in the depletion layer is given by

$$J_{dep} = qF_0[1 - \exp(-aW)]\exp(-ad_n) \tag{39}$$

where F_0 is the light intensity at the front surface of the n-type side, W is the depletion layer width, and d_n is the thickness of the n-type layer from the front surface to the depletion layer edge in the n-type material. Usually contributions to the current generation from the depletion layer and from the n-type material (especially in a heterojunction) are quite small.

IV. Junction Currents

The magnitude of the junction current is, as we have already mentioned, a crucial ingredient in determining the open-circuit voltage and hence the efficiency of a photovoltaic cell. The theory of junction currents in homojunctions is well developed, but this is less true of heterojunctions and MIS or SIS junctions. The subject is so broad that we cannot do more here than give a summary of the major features and mechanisms involved.

A. Homojunctions

Under forward bias in the dark, electrons are injected into the p-type region from the n-type region; they pass from the n-type region where they are majority carriers, through the depletion region, and into the p-type quasi-neutral region where they are minority carriers. In the p-type region they recombine with majority carrier holes, and the current flow is completed by a current of holes from the p-type ohmic contact supplied through the external circuit. Similar statements could be made about the current due to holes; it is sufficient, however, for us to consider specifically just the current due to electrons. If recombination in the depletion region is an important process for the total current generation, in addition to the diffusion process just described, diffusion in the depletion layer is commonly neglected, and the current due to recombination may be calculated and added to the current due to diffusion without recombination in the depletion layer.

1. *Diffusion Currents*

If the electron transport is assumed to be controlled solely by diffusion into the p-type quasi-neutral region with recombination there, with the same being true of hole transport, the current density due to diffusion is given by (*76*)

$$J_{\text{dif}} = qn_i^2[(D_n/\tau_n)^{1/2}/N_A + (D_p/\tau_p)^{1/2}/N_D][\exp(qV/kT) - 1] \quad (40)$$

where n_i is the intrinsic carrier density, N_A is the density of acceptors in the p-type material, and N_D is the density of donors in the n-type material.

2. *Recombination in the Depletion Layer*

An approximate treatment of this case starts with the assumption that the quasi-Fermi levels are constant across the depletion layer. The Shockley–Read recombination model (*77*) indicates that the maximum recombination rate occurs when the intrinsic level lies approximately halfway between the electron and the hole quasi-Fermi levels. The recombination rate $U(x)$ can be replaced by its maximum value by carrying out an integration over the depletion layer to determine the total current carried by recombination. The following approximate expression is obtained for the recombination-controlled current:

$$J_{\text{rec}} = [n_i WkT/2(V_D - V)\tau_{n0}][\exp(qV/2kT) - 1] \quad (41)$$

where W is the depletion layer width, V_D is the diffusion potential of the junction, and τ_{n0} is the minimum lifetime of electrons when all recombination centers are unoccupied. This approximate calculation is the basis for the common contention that $A = 2$ for recombination currents, whereas $A = 1$ for diffusion currents as indicated in Eq. (40). More complete treatments indicate that for recombination currents A is always less than 2 (*76*), a maximum value of 1.8 being predicted for deep recombination centers falling off to 1.0 for shallow recombination centers. The recombination currents in real junctions usually have a larger magnitude than those predicted by available theories to date (*78*). It is also possible to envisage recombination processes corresponding to values of A greater than 2 if recombination occurs through more than one level, or if the levels are distributed nonuniformly in space in the depletion layer (*79*).

B. Heterojunctions

The diffusion injection mechanism for junction currents is usually not the dominant mechanism in heterojunctions. This is partially because most heterojunctions of interest have larger band gaps than silicon does, but also because interface phenomena play such a large role in determining hetero-

junction properties. Several excellent review articles on heterojunctions exist (*45*, *80*, *81*) in addition to the book by Milnes and Feucht (*82*).

Analogous equations to Eqs. (40) or (41) can be written down immediately as approximations to the diffusion or recombination currents expected for a heterojunction with a large-band-gap n-type material on a smaller-band-gap p-type absorber. In general, however, much larger currents are measured. The temperature and voltage dependence of experimentally measured $J-V$ curves appear to fit a variety of semiempirical forms, e.g.,

$$J = J_{00} \exp(-\Delta E/kT)[\exp(qV/AkT) - 1] \tag{42}$$

where J_{00} and A may be slowly varying functions of T and/or V, and ΔE is a measured activation energy for the zero-bias extrapolation of the ln J vs. V curves. In other cases the measured slope of the ln J vs. V curves is relatively independent of temperature but appears again empirically to correspond to a relationship like

$$J = J'_{00} \exp(\beta T) \exp[-\alpha(\phi_b - V)] \tag{43}$$

where β and α are constants that are relatively temperature independent, and $\phi_b = V_D + (E_c - E_f)_n/q$, with $(E_c - E_f)_n$ being the energy distance of the Fermi level below the conduction band edge in the n-type material. In many cases ln J vs. V curves show more than one well-defined region as a function of V. We summarize in the following some of the junction current mechanisms proposed for heterojunctions in addition to the diffusion and recombination analogs to homojunctions.

1. *Direct Recombination through Interface States*

One recombination model for heterojunctions pictures the junction as two Schottky barriers back-to-back on either side of an almost metallic layer of interface states where recombination is very high (*83*, *84*). This model predicts a J vs. V dependence similar to that given by Eq. (42) with a value of A between 1 and 2 depending on the distribution of the depletion layer between the two semiconductors forming the heterojunction. The limiting step in this model is thermal emission of electrons over the barriers at the interface, and hence the model is unable to describe those results found for heterojunctions in which the slope of the ln J vs. V curves are nearly or totally temperature independent.

2. *Transport Control by Interface States*

A similar model has been proposed by Rothwarf (*85*). The limiting step in this case is interfacial recombination characterized by an interface recombination velocity s_i. For the intended case of a Cu_xS/CdS junction where

the Cu_xS is p-type and degenerate, and all of the depletion layer is in the n-type CdS window material, the J vs V relation is given by

$$J(V) = qs_i(n_n - n_{n0}) = qs_iN_D \exp(-qV_D/kT)[\exp(qV/kT) - 1] \quad (44)$$

A value of $A = 1$ is predicted in agreement with experimental results for this type of junction at moderate to high bias voltages under illumination.

3. *Tunneling*

Temperature-independent slopes of the ln J vs. V curves, following Eq. (43), are suggestive of transport by tunneling. Such tunneling is usually appreciable only if the barrier width is less than 100 Å. The tunneling transmission coefficient for normal incidence through the bottom of a triangular barrier of height E_b is (*86*)

$$T(E) = \exp[-4(2m_t^*)^{1/2}E_b^{3/2}/3qh\mathscr{E}] \quad (45)$$

where m_t^* is the tunneling effective mass (*87*, *88*). Considerable crystallographic anisotropy may be introduced through the dependence of m_t^* on crystallographic orientation in suitable materials (*89*).

If a spike exists at the interface (because of electron affinity differences, interface dipoles, and the like), tunneling through this spike may be a controlling factor in junction currents (*80*, *90*). On the other hand, tunneling may also be an important process in materials without a spike if tunneling proceeds from the conduction band of the n-type material. for example, to the valence band of the p-type material via interface or depletion layer imperfection states and a recombination step (*91*). A typical expression for the current resulting from such a combination of tunneling and recombination is given by (*91*)

$$J(V) = BN_t \exp\{[-4(2m_t^*)^{1/2}(V_D - k_2V)]/3hH_0\} \quad (46)$$

with $H_0 = (2qN_A/\epsilon_p)^{1/2}$ and $k_2 = 1/(1 + \epsilon_nN_A/\epsilon_pN_D)$. Here B is a constant containing N_c, the density of tunneling/recombination centers is N_t, ϵ_n and ϵ_p are the dielectric constants of the n- and p-type material. respectively. and k_2 expresses the asymmetry of the junction. It may be seen that Eq. (46) is of the same form as Eq. (43) with a small temperature dependence of J_0 arising from the temperature dependence of the band gaps.

4. *Thermally Assisted Tunneling*

In many heterojunctions behavior is observed in ln J vs. V curves that suggests both tunneling (essentially temperature-independent slope) and thermal activation (current magnitude increasing exponentially with temperature at fixed V). This behavior can be interpreted as resulting from the

effects of thermal excitation necessary to raise carriers to an energy sufficient that tunneling becomes highly probable, whereas tunneling at the bottom of the barrier is not probable. This process of thermally assisted tunneling in Schottky barriers has been considered in some detail by Padovani and Stratton (*92*) and others (*93–96*). The current through the barrier is the integrated product of the incident electron flux and the tunneling transmission probability, both of which are functions of energy. The product has a maximum value centered around some specific energy E_m: For higher energies, the thermal excitation probability decreases exponentially, and for lower energies the tunneling transmission probability decreases exponentially.

Integration was achieved approximately in this problem by Padovani and Stratton by assuming a Gaussian distribution of electron energies about E_m and then by expanding the tunneling integrand in a Taylor's series about E_m. The result is an approximate forward-bias J–V dependence given by

$$J(V) = J_0 \exp(qV/E_0) \tag{47}$$

with

$$E_0 = E_{00} \coth(E_{00}/kT) \tag{48}$$

and

$$E_{00} = (q\hbar/2)(N_D/\epsilon_s m_t^*)^{1/2} \tag{49}$$

for the Schottky barrier case, valid over the range of $kT/4 < E_{00} < 3kT/2$. J_0 in this expression is given by

$$J_0 = \frac{A^* T^2 \pi^{1/2} E_{00}^{1/2} [q(V_D - V)]^{1/2}}{kT \cosh(E_{00}/kT)} \times \exp\{-(E_c - E_f)_n/kT - [q\phi_b - (E_c - E_f)_n]/E_0\} \tag{50}$$

where ϕ_b is the barrier height, and A^* is an adjusted Richardson's constant. At high temperatures and for thick barriers, J_0 is thermally activated with an energy approximately $q\phi_b/A_t$ [if we write Eq. (47) as $J(V) = J_0 \exp(qV/A_t kT)$], whereas at low temperatures and for thin barriers, J_0 is essentially temperature independent.

This treatment has been extended to heterojunctions by Tansley and Owen (*97*), who did a computer calculation for a parabolic potential barrier, using the WKB approximation for the tunneling transmission probability. Excellent agreement was found for a variety of heterojunctions between p-GaAs and n-Ge, n-$Ga_xIn_{1-x}As$, and n-$GaAs_yP_{1-y}$. The simple Schottky barrier form of Padovani's theory has also been applied with some success to a ZnO/CdTe heterojunction, consisting of a degenerate ZnO n-type layer on a p-type single crystal p-type CdTe substrate (*59*). In this case electrical measurements as well as the tunneling behavior indicated that a high

density of charged deep acceptors within the depletion layer reduced the width of a portion of the depletion layer sufficiently to allow thermally assisted tunneling.

C. Schottky Barriers

Schottky barriers share many of the same transport mechanisms controlling the junction current in homojunctions and heterojunctions. The forward-bias junction current mechanisms have been reviewed by Rhoderick (*95*) and Padovani (*96*), and they include thermionic emission of electrons from the semiconductor into the metal over the Schottky barrier, recombination in the depletion region, tunneling through the barrier, and minority carrier injection and diffusion. The properties of a Schottky barrier can be viewed as the limiting case of a heterojunction when the interface recombination velocity becomes infinite.

The usual dominant transport mechanism in Schottky barriers is simple thermionic emission over the barrier. This was treated some years ago by Bethe (*98*) with the result that

$$J = A^*T^2 \exp(-\phi_b/kT)[\exp(qV/kT - 1)] \tag{51}$$

with $q\phi_b = qV_D + (E_c - E_f)_n$ as usual and

$$A^*T^2 = 4\pi qm^*k^2T^2/h^3 = qN_c(kT/2\pi m^*)^{1/2} \tag{52}$$

For $m^* = m$, A^* is 120 A/cm^2 K, the normal Richardson constant for thermionic emission into vacuum. Corrections may be needed for field lowering of the potential barrier for thin barriers (*99*) and surface state effects (*100*).

The above calculations are based on the assumption that the Fermi level is constant throughout the depletion layer. The Fermi level may be expected to be lowered slightly near the interface if the electron mean free path is less than the depletion layer width, so that transport is limited by the diffusion of the carriers (*101*). Crowell and Sze (*99, 102*) have combined the thermionic emission theory of Bethe and the diffusion theory of Schottky, and to this added electron–phonon interactions, quantum mechanical transmission of the barrier, and image force lowering to form a single model. Their results indicate that with slight modifications Eq. (51) adequately describes the junction current for all except very thin barriers where tunneling cannot be neglected.

D. MIS Junctions

Unless Schottky barriers are prepared under the most scrupulous of conditions, the existence of a thin oxide layer between the metal and the

semiconductor is a common occurrence. Since this oxide layer can have beneficial results, efforts are sometimes made to grow such layers in a controlled fashion to improve junction performance.

An insulating layer between the metal and the semiconductor of an MIS junction may do the following: (*a*) act as a dielectric separating the metal and semiconductor, thereby decreasing the barrier heights; (*b*) limit the flow of carriers, since transport through the insulating layer is either by tunneling or by space-charge-limited currents, thereby reducing the current flow for a given applied voltage; (*c*) partially sustain the applied voltage, thus leading to variation in barrier height with voltage and diode factors A greater than unity; and (*d*) further increase or decrease the effective barrier height because of trapped charge within the insulating layer or at the insulator–semiconductor interface, depending on the sign of the charge.

The dark current in an MIS diode is the sum of four components as pictured in Fig. 14: J_{th}, thermionic emission over the barrier; J_{rg}, recombination/generation in the depletion layer; J_{id}, injection and diffusion into the quasi-neutral bulk; and J_{s}, recombination at the semiconductor–insulator interface. All currents, of course, must tunnel through the insulating layer. The presence of the insulating layer can decrease the magnitude of the majority carrier current J_{th} so that it becomes comparable to the minority carrier currents J_{rg} and J_{id}, thus producing a substantial increase in the open-circuit voltage. The maximum thickness of the insulating layer is

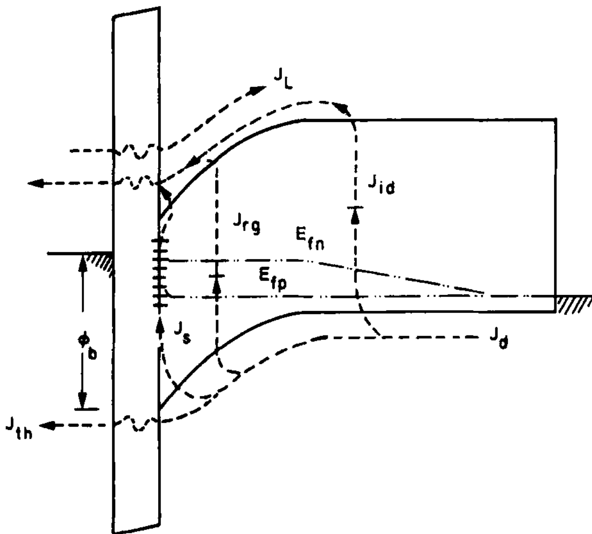

FIG. 14. Current flow routes in an MIS junction for forward bias of a p-type semiconductor. Quasi-Fermi levels are shown for the dark case.

controlled by the necessity for light-generated carriers to tunnel through this layer also, and an optimum thickness of 20 to 30 Å is usually found.

From Eq. (51) if we generalize slightly to include specifically a diode factor A that need not be exactly unity, the open-circuit voltage for a Schottky barrier controlled by thermionic emission currents is given by

$$V_{oc} = A\phi_b + (AkT/q)\ln(J_{sc}/A^*T^2) \tag{53}$$

This expression is still valid for the MIS device, provided that actual values of ϕ_b and A are used, and that the insulating layer is thin enough to allow free tunneling. Examination of Eq. (53) shows that the value of V_{oc} can be increased by the insulating layer if its presence serves to increase either ϕ_b or A. A variety of models have been proposed that describe such possibilities (*103–112*).

E. SIS Junctions

Because actual heterojunctions often show large values of J_0 which result in a decreased value of V_{oc}, the inclusion of a thin insulating layer between the two semiconductors may be expected to have the same kind of beneficial effect as such a layer between the metal and semiconductor of a MIS junction. Many systems, especially those in which one of the members of the heterojunction is a conducting oxide, might be expected to have such an oxide layer as a matter of course. Analysis of the situation is complex, and an analysis by DeVisschere and Pauwels (*113*) indicates that the presence of an insulating layer may be disadvantageous if photogeneration of carriers occurs primarily in the more heavily doped semiconductor, but advantageous if photogeneration occurs primarily in the less heavily doped semiconductor. An SIS model has been proposed to describe the indium–tin oxide heterojunction with silicon (*114*).

V. Examples of Photovoltaic Materials Systems

It is an exaggeration (albeit not without considerable truth) to say that a junction between any two materials will show a measurable photovoltaic effect except in very special cases. To show a large enough photovoltaic effect to be of general practical interest, e.g., to have a conversion efficiency for solar radiation of at least 10%, is quite another matter. In fact to date only six materials have produced such high efficiencies: silicon, gallium arsenide, indium phosphide, cuprous sulfide, cadmium telluride, and copper indium selenide. Bucher (*15*) has given an extensive summary of many different types of photovoltaic systems for which basic parameters have been

reported. In this review we seek only to give a perspective on the types of systems that have shown considerable promise.

A. Silicon

The Si p–n junction cell is at the present time the only practical solar cell widely available commercially. Reviews of the technological development of the silicon cell have been written by Wolf (*115*) and Brandhorst (*116*). These developments have increased the efficiency of single crystal p–n junction silicon cells to values in the range of 15–17%. Improvements have come about by detailed refinements directed toward the solution of particular problems, e.g., an increase in the blue-violet response of the cell by decreasing the thickness of the front n-type layer and increasing its minority carrier diffusion length to produce the "violet cell," (*117*) and the introduction of a back surface field to decrease loss at the back surface of the cell (*118*). Standard single crystal growth methods have in recent years been supplemented by methods aimed at reducing the cost of slicing and polishing wafers from grown crystals by producing thin ribbons of Si directly (*119–121*).

1. *Single Crystal* p–n *Junctions*

The band diagram of a typical Si single crystal p–n junction is given in Fig. 15. The cell consists of single crystal Si 200–500 μm thick with p-type conductivity. The n-type layer is about 0.1–0.5 μm thick and is produced by diffusion of P or As donor impurities. The back contact typically consists of Al, deposited by vacuum evaporation and heat-treated to produce a p^+ region capable also of acting as a back surface field. A three layer Ti/Pd/Ag contact is used to the front surface in the form of a suitable grid.

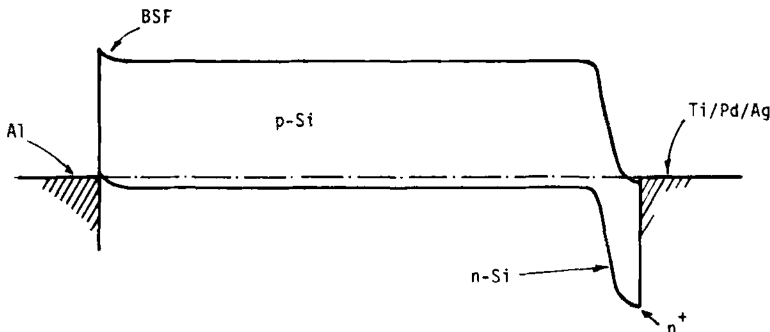

FIG. 15. Energy band diagram for a typical Si homojunction p–n junction photovoltaic cell. The thickness of the n-type layer is exaggerated.

The 400-Å Ti layer acts to produce a strong mechanical bond between Ag and Si, and the 200-Å Pd layer inhibits a possible electrochemical reaction between Ti and Ag in the presence of moisture. The front surface grid usually covers about 5–10% of the total area. To reduce the reflectivity of Si (33–54% on a bare surface over the range of 0.35–1.1 μm) antireflection coatings must be used. Materials such as SiO, SiO_2, Si_3N_4, Al_2O_3, TiO_2, and Ta_2O_5 have been used as antireflection coatings; one such layer can reduce the reflectivity over the spectral range of interest to 10%, while two layers can reduce it to 3%. Surface texturing has also been used to reduce the reflectivity of silicon (*122*).

An example of a highly developed cell is the "COMSAT nonreflective" cell, which makes use of a texturized surface to reduce reflection and allow light to travel in paths that are not perpendicular to the junction interface (*117*). This cell has $V_{oc} = 0.59$ V, $J_{sc} = 46$ mA/cm^2, and a fill factor of 0.78 to yield an efficiency of 15.5% for space radiation conditions. The value of J_0 is 6×10^{-12} A/cm^2. Under terrestrial radiation conditions, it is expected that this cell will have $J_{sc} = 34$ mA/cm^2 and an efficiency of about 18%.

2. *Polycrystalline Silicon*

A considerable savings in production cost would be achieved if polycrystalline silicon could be used in place of the single crystalline material just described (*21*). In general such cells have a lower efficiency but allow many fabrication steps to be eliminated. Polycrystalline silicon can be used in a variety of cell designs, including p–n junction, Schottky barrier, and MIS structures. Large-grain polycrystalline Si cells have been made by directional solidification casting, which produces mm-size grains and a columnar structure with single-crystal-like properties in the direction of the incident light; efficiencies of the order of 12% have been reported (*123*). Lindmayer (*124*) has reported polycrystalline cell efficiencies up to 16%.

Diffusion formation of p–n junctions on polycrystalline silicon is complicated by the tendency of the dopant to diffuse rapidly down grain boundaries. Schottky barrier and MIS cells formed by vacuum evaporation of the other layers on polycrystalline silicon or the use of ion implantation doping avoid this difficulty to some extent.

3. *Silicon MIS Junction*

MIS junction cells on silicon have been developed with efficiency comparable to the best single-crystal p–n junction cells. Such cells with efficiencies between 8 and 12% were made fairly early using Cr/SiO_2/p-Si (*125*, *126*), Al/SiO_2/p-Si (*127*), and Au/SiO_2/n-Si (*128*).

The inversion layer MIS cells is an example of an interesting variation of the MIS structure. The charge in the insulating layer next to the semiconductor interface is strong enough to actually form an inversion layer in the semiconductor surface, thus producing an n–p homojunction via the n–type inversion layer on p–type silicon (*129*). Godfrey and Green (*130*) have reported an efficiency of 17.6% for such a cell using either Mg or Al as the metal. It has been shown that the junction current in this case is minority carrier dominated.

4. *Silicon Junctions with Conducting Metal Oxides*

Efficient cells have been prepared from junctions of silicon with high band gap conducting oxides such as SnO_2, In_2O_3 or solid solutions of indium–tin oxides (ITO) as the n-type window material. These oxides are almost completely transparent in the visible portion of the spectrum, while being degenerate semiconductors at the same time. There is considerable evidence that they should be regarded as SIS junctions rather than as simple heterojunctions (*114*), especially the observation that equally efficient cells can apparently be made on both p-type and n-type silicon (*131*, *132*). An SnO_2/n-Si cell in which the SnO_2 was deposited by electron beam evaporation and the insulating layer was formed by a subsequent annealing in air showed an efficiency of 10–12% (*133*). An ITO/p-Si cell that showed an efficiency of 12.8% was analyzed in terms of an SIS model (*114*, *131*). Such oxide/Si junctions have tended to show a degradation in performance with time, presumably owing to the growth in thickness of the insulating oxide layer (*134*). Overall implications of this degradation mechanism for ultimate practical utility of this type of cell are uncertain.

5. *Amorphous Silicon*

Amorphous silicon, or more specifically amorphous hydrogenated silicon, a-Si:H, initially prepared by the glow discharge decomposition of silane, SiH_4 (*135*), and containing approximately 20–30% of hydrogen, represents a relatively new form of silicon which is of considerable interest (*21*). Differences between the a-Si:H and single crystal Si are most evident in the optical absorption spectrum; the absorption constant is appreciably increased in the a-Si:H material, which exhibits behavior such as a direct band gap at 1.55 eV rather than the indirect band gap at 1.1 eV characteristic of crystalline silicon (*136*). Hydrogenation apparently decreases the density of localized states by satisfying the broken bonds in the amorphous silicon, thus making possible the doping of the amorphous material n- and p-type (*137–141*).

The behavior of a-Si:H as a solar cell material, however, is considerably different from that of single crystal Si, since a-Si:H has a relatively high resistivity and a low carrier mobility. Doping of the a-Si:H to reduce the resistivity produces very short carrier diffusion lengths. Attempts have been made to use the a-Si:H in solar cells using heterojunction, p–i–n, and Schottky barrier structures (*136*, *142–144b*). The following design trade-off is encountered: Since the a-Si:H has short diffusion lengths, it is desirable to have the depletion layer extend over as wide a region as possible, so that the drift field can be used to help collect photogenerated carriers; i.e., it is desirable to have high-resistivity material, but, on the other hand, high-resistivity material contributes to the series resistance of the cell. Two other complications arise: (*a*) since the depletion layer width is a function of forward bias, the width of the field-controlled region changes with voltage; and (*b*) since a-Si:H is photoconductive, illumination changes the diffusion voltage of the junction.

The most efficient cells prepared from a-Si:H have been of the p–i–n barrier type, yielding $V_{oc} = 0.86$ V, $J_{sc} = 13.0$ mA/cm^2, ff = 0.62, and efficiency of 6.9% (*144b*). Great interest in a-Si:H solar cells persists, since this material provides a way of producing large-area cells at low cost. Although a maximum feasible efficiency of about 15% may be estimated, it remains to be seen whether practical problems can be overcome in real cells to allow the efficiency to increase appreciably beyond its present values in stable and reproducible cells.

B. Gallium Arsenide

The band gap of GaAs at 1.43 eV is near the optimum for solar energy conversion as a photovoltaic material, with a theoretical efficiency of 26–29% for terrestrial use. In addition GaAs has a direct band gap and can absorb 97% of the solar radiation received at the earth's surface within about 2 μm thickness. Although GaAs p–n homojunctions can be prepared (*145*, *146*), their performance is limited by high front-surface recombination as is typical of a direct band gap homojunction. A major advance occurred when Alferov *et al.* reported the first p-AlGaAs/n-GaAs heterojunction structure with a space efficiency of 10–11% and a strongly increased short-wavelength response compared to a p–n homojunction (*147*). A second major increase in efficiency occurred with the introduction of the heteroface p-AlGaAs/p-GaAs/n-GaAs structure in 1972 fabricated by liquid-phase epitaxy techniques, which had an efficiency of 15.3% for terrestrial radiation and 19.1% in space (*148*). Although an n^+–p homojunction layer with a 0.045-μm thick front n^+ layer was reported to have a terrestrial efficiency of 20% after

passivation of the front surface by anodization (*149*), heteroface structures still hold the lead in efficiency, with values of about 21–22% being reported without concentration (*150, 151*), and a value of 24.7% for a concentration factor of 180 (*152*).

The good performance of the heteroface structure can be traced to the good lattice constant match between AlGaAs and GaAs, producing a low density of interface states at the heteroface interface, corresponding to an interface recombination velocity of less than 10^4 cm/sec (*153*). At the front surface of the AlGaAs the surface recombination velocity is still high, of the order of 10^6 cm/sec, but because of the large indirect band gap of AlGaAs, only a small fraction of the light current is generated in the AlGaAs layer.

The junction current vs. voltage behavior of GaAs cells is remarkably well described in terms of the basic injection and recombination transport mechanisms. Particularly at high concentration factors for the radiation, most cells show $A = 1$ with values of J_0 reported to be as low as 10^{-19} A/cm^2 (*154*).

Because of the high cost of the material itself and because of the precision fabrication processes required to produce these high-efficiency single crystal cells, their major application is in the area of concentrator systems, where concentration of the sunlight by a particular factor allows an increase in cost by roughly the same factor over a cell to be used without concentration (*155*). Efficiency usually increases with concentration, and concentration factors in excess of 10^3 are favored. Under these conditions extreme care must be taken to maximize current collection, since total series resistance values of less than 10^{-3} $\Omega \cdot$cm^2 are required. For a typical heteroface cell fabricated for use with concentration, the following parameters are reported for concentration of terrestrial radiation by a factor of 10^3: $J_{sc} = 23.7$ A/cm^2, $V_{oc} = 1.19$ V, efficiency = 20% (*154*).

Schottky barrier and MIS cells have also been prepared using GaAs single crystals. The presence of an insulating layer plays an important role in improving the performance of Schottky barriers. Figure 16 shows the dramatic effect on the open-circuit voltage of various stages of oxidation on an n-GaAs surface before application of a gold Schottky barrier contact. The effect is not exactly that expected from our previous considerations; increasing insulating layer thickness is actually accompanied by an increase in J_0, but an accompanying increase in A more than compensates for this increase in J_0 and produces a net increase in V_{oc} (*156*). The type of cell shown in Fig. 16 has been called an AMOS cell (antireflection-coated metal–oxide–semiconductor), and efficiencies up to 15% were measured corresponding to these data. As indicated by Eq. (53) two factors play a role in the effect of an oxide layer on the properties of an Au/GaAs MIS junction: increases in

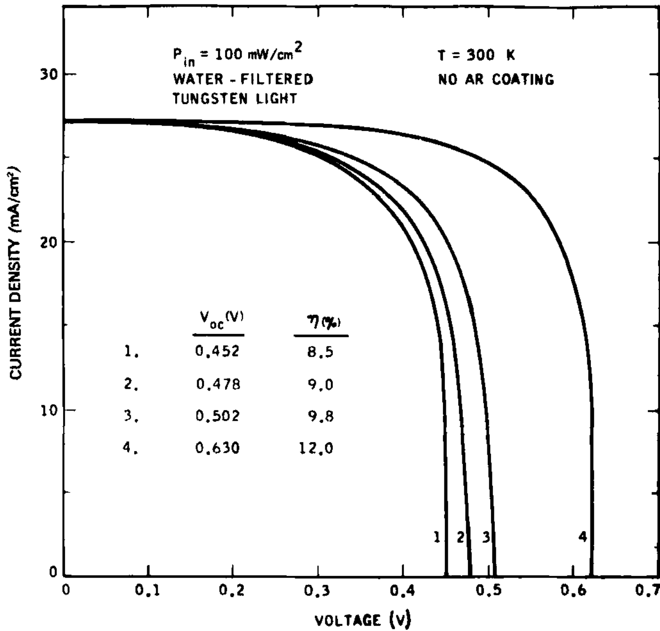

FIG. 16. Light current–voltage curves for Au/GaAs MIS junctions for various treatments of the GaAs surface before application of the metal barrier contact. (1) "Clean" interface, $V_{oc} = 0.452$ V, $\eta = 8.5\%$; (2) exposed to air at 300 K for 4 hr, $V_{oc} = 0.478$ V, $\eta = 9.0\%$; (3) exposed to air at 300 K for 94 hr, $V_{oc} = 0.502$ V, $\eta = 9.8\%$; and (4) exposed to air at 403 K for 70 hr, $V_{oc} = 0.630$ V, $\eta = 12.0\%$. [From Stirn and Yeh (*156*).]

barrier height or increases in A, as was the case for the Si MIS devices. The effect is also quite sensitive to the specific crystal orientation of the GaAs face which is oxidized or on which the oxide layer is deposited.

The insulating layer in an MIS device need not always be an oxide. Equivalent results have been reported for an Au/n-AlGaAs/n-GaAs cell, in which the n-AlGaAs is a 500-Å thick layer made highly resistive by depletion (*157*). The magnitude of V_{oc} increases with Al mole fraction x, from 0.53 V for $x = 0$ to 0.70 V for $x = 0.5$; a conservative estimate suggests that an efficiency of 19.5% should be possible on an optimized cell of this type.

C. Cu_xS/CdS Thin-Film Heterojunctions

From the late 1950s and for a period of almost 20 years the only all thin-film photovoltaic cell available was that formed from a heterojunction between p-type Cu_xS and n-CdS, where for the best photovoltaic performance x lies between 1.995 and 2.000, corresponding to the chalcocite structure

of Cu_xS. The p-type Cu_xS has a band gap of about 1.2 eV and is the absorber member of the junction; n-type CdS has a band gap of about 2.4 eV and is the large-band-gap window material.

The cells of this type have characteristics of the most simple and the most complex of systems. Simplicity lies in the fact that a thin film of CdS deposited, for example, by vacuum evaporation or spray pyrolysis, needs simply to be dipped for a brief period into a warm aqueous solution containing cuprous ions to form a topotaxial layer of Cu_xS by a replacement reaction. Other methods may be used, the most popular of which is the vacuum evaporation of CuCl onto CdS, followed by a heat treatment to form the Cu_xS and a washing to remove $CdCl_2$. Complexity arises because there is appreciable lattice mismatch between the two materials, Cu diffusion into the CdS occurs near the interface producing the depletion layer in the window material rather than in the absorber, a variety of Cu_xS phases exist at room temperature with quite different photovoltaic properties, and the usual grain boundary effects are present owing to the polycrystalline materials.

The historical development of the understanding of the mechanisms of the Cu_xS/CdS cell had an interesting if tortuous record (*6*, *158–174*). The unified model of the Cu_xS/CdS heterojunction has the following general characteristics: (*a*) light absorption in the Cu_xS dominates current generation: (*b*) the forward junction current flows primarily via recombination through interface states; (*c*) diffusion of Cu into the CdS widens the depletion layer in the lower carrier-density n-type CdS, giving rise to localized states whose charge can be modulated by illumination; (*d*) low-energy photon response is enhanced by high-energy photon illumination because of the effects on the junction width through modulation of this charge in localized states near the interface; (*e*) dark and light forward-bias J–V curves commonly cross owing to effects of illumination on junction current mechanisms; (*f*) long-term loss of sensitivity may be caused by changes in the Cu_xS composition or by additional diffusion of Cu into the CdS; and (*g*) control of the injection of photoexcited carriers from the Cu_xS into the CdS and the injection of carriers from the CdS into the Cu_xS under forward bias occurs via recombination or tunneling/recombination through interface states (*175*, *176*) rather than via a series photoconducting layer of insulating CdS:Cu (*174*) or a small conduction band spike between the Cu_xS and the CdS (*177–179*).

Development of the Cu_xS/CdS cell in recent years has been carried forward with some success at the Institute for Energy Conversion of the University of Delaware (*7*). The heterojunction itself consists of about 20 μm polycrystalline CdS and 0.3 μm of Cu_xS. The penetration of Cu_xS down grain boundaries in the CdS yields a highly three-dimensional layer; this effect is avoided by using the evaporation of CuCl rather than the dipping

process to form the Cu_xS. Best photovoltaic parameters reported to date are $V_{oc} = 0.52$ V, $J_{sc} = 21.8$ mA/cm^2, ff = 0.71, yielding an efficiency of 9.14% for terrestrial radiation.

A materials variation that might be expected to improve the performance of Cu_xS/CdS cells would be the partial substitution of Zn for Cd to form a $Zn_yCd_{1-y}S$ solid solution (*7*). Such a substitution would be expected on first principles to produce both a larger V_{oc} because of the electron affinity change and also a larger J_{sc} because of the larger-band-gap window. The bulk resistivity of $Zn_yCd_{1-y}S$ increases rapidly with increasing y, so that practical values of y are probably limited to less than 0.20 (*180–182*). Measurements on dipped $Cu_xS/Zn_{0.18}Cd_{0.82}S$ cells did show an increase in open-circuit voltage $V_{oc} = 0.60$ V, but a slightly decreased $J_{sc} = 15.8$ mA/cm^2, yielding an efficiency of 7.4%. Subsequent research has produced a cell with efficiency greater than 10%.

D. Indium Phosphide

Indium phosphide is in many ways similar to GaAs; it has a direct band gap of 1.34 eV, is limited in homojunction form by surface recombination, and should function well in heterojunctions. As a semiconductor material, however, InP has not received to date the technological development accorded to Si or even to GaAs.

A nearly ideal heterojunction is possible with n-CdS and p-InP, since the lattice constant match between these two materials is very close (*60–62, 183, 184*). Cells with high efficiency up to 15% have been fabricated by vacuum evaporation, chemical vapor deposition, and close-spaced vapor transport deposition of CdS onto single crystal InP substrates. Problems with polycrystalline InP substrates have been described in Section II,D,9.

The most efficient CdS/InP cells were made by using a chemical vapor deposition method for depositing CdS on InP using an open-tube H_2S/H_2 flow system (*60–62*). Apparently the presence of about 2 mol % of H_2S in the gas flow serves to continuously etch the surface of the InP by the formation and sublimation of indium sulfides; thus CdS nucleates on a clean surface and prevents further attack of the InP by the H_2S. Cell parameters measured were $V_{oc} = 0.79$ V, $J_{sc} = 18.7$ mA/cm^2, ff = 0.74, yielding an efficiency of 15.0%.

The largest value of V_{oc} for a CdS/InP heterojunction was produced by the close-spaced vapor transport deposition of CdS (*185*). An open-circuit voltage of 0.81 V was obtained in a 14.4% efficient cell.

In view of this argument that the high efficiencies realized for CdS/InP junctions were the result of good lattice match and clean InP surfaces, it is

surprising to find that equally efficient cells can be prepared with ITO/InP junctions in which the ITO is deposited either by ion-beam deposition methods (*186*) or by sputtering (*187–190*). The resolution of this apparent dilemma was given by the realization that in all cases of high-efficiency ITO/InP junctions, it is highly likely that a heteroface buried junction has been formed either by diffusion of a donor like tin from the ITO or simply by sputtering-induced damage of the InP surface.

E. Cadmium Telluride

Of the six chalcogenide compounds of Zn and Cd, only CdTe can be made highly conducting in both n- and p-type forms. CdTe is the II–VI analog of the III–V materials GaAs and InP; it has a direct band gap of about 1.50 eV. Like these direct-band-gap materials, homojunctions of CdTe are limited by high front surface recombination losses to values of the order of 8% (*191–194*). Schottky barrier cells, Pt/n-CdTe, and Au/n-CdTe have been fabricated (*195*). However, heterojunctions involving CdTe or heteroface buried junctions in CdTe appear to be the most promising.

Vacuum evaporation of CdS onto single-crystal CdTe produced a heterojunction with an efficiency of 8% and the spectral response shown in Fig. 8 (*196*). Chemical vapor deposition of CdS onto single-crystal CdTe was reported to produce cells with efficiency as high as 12% (*197*, *198*), although the evidence in this case indicates that a heteroface buried junction has been formed by n-type impurities from the CdS diffusing into the CdTe during deposition. Both CdS/CdTe and ZnCdS/CdTe junctions have been prepared by spray pyrolysis deposition of the CdS or ZnCdS with efficiencies in the 6–8% range (*199*, *200*). An efficiency of 8% is also reported for a heteroface CdS/CdTe cell produced by the simple method of screen printing; this cell had the complex structure represented by n-CdS/n-CdTe/p-CdTe:Cu/p-Cu_xTe (*201*).

Large-band-gap conducting oxides such as ITO and ZnO are also attractive as window materials for use in heterojunctions. Both of these materials have been used with CdTe. An ITO/CdTe junction formed by sputtering of ITO proved to be a heteroface buried junction with an efficiency of 8% (*202*). On the other hand, a ZnO/CdTe junction formed by spray pyrolysis deposition of ZnO onto single crystal CdTe showed a genuine heterojunction response with an efficiency of about 9% (*59*).

F. $CuInSe_2$

$CuInSe_2$ is the fifth material mentioned at the beginning of Section V that has been made in some form to produce an efficiency of over 10%. It is a struc-

turally more complex material, belonging to the family of I–III–VI_2 chalcopyrites. $CuInSe_2$ has a direct band gap of 1.04 eV, somewhat smaller than most of the absorbing materials used in solar cells. However, its chalcopyrite structure yields a lattice constant that is a good match with CdS. CdS/$CuInSe_2$ junctions prepared by vacuum evaporation of CdS onto single crystal p-type $CuInSe_2$ and fitted with an SiO antireflection coating showed $V_{oc} = 0.49$ V, $J_{sc} = 38$ mA/cm^2, ff = 0.60, yielding an efficiency of 12% (*202*, *203*).

All thin-film junctions of CdS/$CuInSe_2$ have also been investigated, and the best cells show a heterojunction-like response with $V_{oc} = 0.40$ V, $J_{sc} =$ 39 mA/cm^2, ff = 0.63, and an efficiency of 9.5% (*204–206b*).

G. Other Possible Materials of Promise

In spite of the promise shown by the major binary compounds of III–V and II–VI types for the production of solar cells, it is still hoped that some other compound might be found that would be structurally simple, composed of abundant elements, capable of inexpensive fabrication into solar cells, and able to display high efficiency for solar energy conversion, which might have some ultimate advantage over the better-known materials.

One binary compound that has emerged from such a search is Zn_3P_2 (*207*). It has a band gap of about 1.4 eV and can readily be prepared in single crystal or thin-film form with p-type conductivity. No isolated n-type form of the material is known to date. Mg/Zn_3P_2 junctions, for which some evidence exists that a buried homojunction has been formed rather than a simple Schottky barrier, have been prepared with an efficiency of 6.0% on bulk polycrystalline Zn_3P_2 (*208*). The same investigators have produced a 2.7% efficient all thin-film Mg/Zn_3P_2 cell, and a 2% ZnO/Zn_3P_2 cell prepared by sputtering of ZnO.

Other materials of exploratory interest are $ZnSnP_2$, $ZnSiAs_2$, and $CdSiAs_2$. Research continues on Cu_2O, one of the first of the photovoltaic materials, without major improvement in efficiency. Schottky barrier cells of Al/p-WSe_2 have yielded 5.3% efficiency (*209*); this material has a direct band gap of 1.35 eV and can be made in either n- or p-type form.

If the quest for a simple binary compound is extended to other materials, one may wish to consider the possibility of controlled multielement solid solutions so that both lattice constant match and desirable band gap can be simultaneously achieved (*210–212*).

Polymeric $(SN)_x$ with a high anisotropic dc conductivity when properly prepared apparently has a larger work function than the elemental metals (*213*); this material might therefore be of interest as a Schottky barrier

material with suitable semiconductors, or as an ohmic contact to p-type materials for which no metals exist with large enough work function to provide such contacts. Experimental cells of $(SN)_x$/n-GaAs have been prepared with 6% efficiency (*214*). Other polymers such as polyacetylene, $(CH)_x$, may be of interest; $(CH)_x$ itself has a band gap of about 1.6 eV and can be doped either n- or p-type, but performance of cells using it appear to be limited by short diffusion lengths for the minority carriers (*215*). Organic materials can, in principle, be used as the absorber material in a photovoltaic cell, but results to date indicate low efficiencies because of short minority carrier diffusion lengths and high series resistance (*216*, *217*).

REFERENCES

1. E. Becquerel, *Compt. Rend.* **9**, 561 (1839).
2. W. C. Adams and R. E. Day, *Proc. R. Soc.* **A25**, 113 (1877).
3. W. Smith, *Nature* (*London*) 7, 303 (1873).
4. D. M. Chapin, C. S. Fuller, and G. L. Pearson, *J. Appl. Phys.* **25**, 676 (1954).
5. D. A. Jenny, J. J. Loferski, and P. Rappaport, *Phys. Rev.* **101**, 1208 (1956).
6. D. C. Reynolds, G. Leies, L. L. Antes, and R. E. Marburger, *Phys. Rev.* **96**, 533 (1954).
7. A. Rothwarf and A. M. Barnett, *IEEE Trans. Electron. Dev.* **ED-24**, 381 (1977).
8. H. Hovel, "Semiconductors and Semimetals," Vol. 11. Academic Press, New York, 1975.
9. C. E. Backus, ed., "Solar Cells." IEEE Selected Reprint Series, Wiley (Interscience), New York, 1976.
10. J. A. Merrigan, "Sunlight to Electricity." MIT Press, Cambridge, Massachusetts, 1975.
11. H. W. Brandhorst and M. P. Godlewski, eds., *IEEE Trans. Electron. Devices*, **ED-24**, No. 4 (1977).
12. R. C. Neville, "Solar Energy Conversion: The Solar Cell." Elsevier, New York, 1978.
13. W. Palz, "Solar Electricity." Butterworths, London, 1978.
14. D. L. Pulfrey, "Photovoltaic Power Generation." VanNostrand-Reinhold, New York, 1978.
15. E. Bucher, *Appl. Phys.* **17**, 1–25 (1978).
16. E. W. Williams, ed., *IEE J. Solid-State and Electron Devices*, **2** (1978).
17. H. Ehrenreich, chairman. "Principal Conclusions of the American Physical Society Study Group on Solar Photovoltaic Energy Conversion." American Physical Society, New York, January (1979).
18. B. O. Seraphin, ed., *Top. Appl. Phys.* **31** (1979).
19. F. A. Lindholm and P. Rappaport, eds., *IEEE Trans. Electron Devices* **ED-27**, 613 (1980).
20. T. Coutts, L. L. Kazmerski, and S. Wagner, eds., Photovoltaic Material and Device Measurement Workshop, Solar Cells, Vol. 1, Nos. 2 and 3.
21. H. K. Charles, Jr., and A. P. Ariotedjo, *Sol. Energy* **24**, 329–339 (1980).
22. E. A. Perez-Albuerne and Y.-S. Tyan, *Science* **208**, 902–907 (1980).
23. S. Fonash, "Solid State Energy Conversion." Academic Press, New York, 1981.
24. A. L. Fahrenbruch and R. H. Bube, "Fundamentals of Solar Cells," Academic Press, New York, 1981.
25. T. Piwkowski, *Acta Phys. Pol.* **15**, 271 (1956).
26. G. Schwabe, *Z. Naturforsch.* **10a**, 78 (1955).

27. J. Starkiewicz, L. Sosnowski, and O. Simpson, *Nature* (*London*) **158,** 28 (1946).

28. R. Y. Berlaga and L. P. Strakhov, *Zhr. Tekh. Fiz. USSR* **24,** 943 (1954).

29a. L. Pensak, *Phys. Rev.* **109,** 601 (1958).

29b. B. Goldstein, *Phys. Rev.* **109,** 601 (1958).

30. B. Goldstein and L. Pensak, *J. Appl. Phys.* **30,** 155 (1959).

31. S. G. Ellis, F. Herman, E. E. Loebner, W. J. Merz, C. W. Struck, and J. G. White, *Phys. Rev.* **109,** 1860 (1958).

32. G. Cheroff and S. P. Keller, *Phys. Rev.* **111,** 98 (1958).

33. C. F. Neumark, *Phys. Rev.* **125,** 838 (1962).

34. R. M. Swanson, *Proc. IEEE* **67,** 446 (1979).

35. H. Gerischer, *Top Appl. Phys.* **31** (1979).

36. W. D. K. Clark and J. A. Eckert, *Sol. Energy* **17,** 147 (1975).

37. R. L. Anderson, *Solid State Electron.* **5,** 341 (1962).

38. H. J. Hovel, J. M. Woodall, and W. E. Howard, *Symp. GaAs, Boulder, Inst. Phys. Phys. Soc.* (*London*), p. 205 (1972).

39. I. Lindau, P. W. Chye, C. M. Garner, P. Pianetta, C. Y. Su, and W. E. Spicer, *J. Vac. Sci. Technol.* **15,** 1332 (1978).

40. W. E. Spicer, I. Lindau, P. E. Gregory, C. M. Garner, P. Pianetta, and P. W. Chye, *J. Vac. Sci. Technol.* **13,** 780 (1976).

41. A. Huijser and J. van Laar, *Surf. Sci.* **52,** 202 (1975).

42. J. E. Rowe, S. B. Christman, and G. Margaritondo, *Phys. Rev. Lett.* **35,** 1471 (1975).

43. G. Margaritondo, S. B. Christman, and J. E. Rowe, *Phys. Rev. B* **14,** 5396 (1976).

44. J. E. Rowe, G. Margaritondo, and S. B. Christman, *Phys. Rev. B* **15,** 2195 (1977).

45. A. L. Fahrenbruch and J. Aranovich, *Top. Appl. Phys.* **31** (1979).

46. J. P. Donnelly and A. G. Milnes, *Int. J. Electron.* **4,** 295 (1966).

47. K. W. Mitchell, A. L. Fahrenbruch, and R. H. Bube, *J. Appl. Phys.* **48,** 4365 (1977).

48. A. Rothwarf, Tech. Rep. NSF/RANN/AER 72-03478 A04/TR 76/1. Institute of Energy Conversion, Newark, Delaware, 1976.

49. M.-J. Tsai and R. H. Bube, *J. Appl. Phys.* **49,** 3397 (1978).

50. R. L. Petritz, *Phys. Rev.* **104,** 1508 (1956).

51. D. E. Riemer, *IEEE Photovolt. Spec. Conf. 13th, Proc.*, p. 603 (1978).

52. M. Wolf and H. Rauschenbach, *Adv. Energy Conv.* **3,** 455 (1963).

53. C. R. Fang and J. R. Hauser, *IEEE Photovolt. Spec. Conf., 13th, Proc.*, p. 1306 (1978).

54. K. W. Heizer and T. L. Chu, *Solid State Electron.* **19,** 471 (1976).

55. D. W. Spaderna and D. H. Navon, *IEEE Trans. Electron Devices* **ED-25,** 1290 (1978).

56. K. W. Mitchell, *IEEE Electron Devices Conf., Washington, D.C.*, p. 229 (1977).

57. J. J. Loferski, *J. Appl. Phys.* **27,** 777 (1956).

58. N. B. Urli, U. V. Desnica, and E. Coffou, *IEEE Trans. Electron Devices* **ED-22,** 1077 (1975).

59. J. Aranovich, D. Golmayo, A. L. Fahrenbruch, and R. H. Bube, *J. Appl. Phys.* **51,** 4260 (1980).

60. J. L. Shay, S. Wagner, M. Bettini, K. J. Bachmann, and E. Buehler, *IEEE Trans. Electron Devices* **ED-24,** 483 (1977).

61. M. Bettini, K. J. Bachmann, E. Buehler, J. L. Shay, and S. Wagner, *J. Appl. Phys.* **48,** 1603 (1977).

62. M. Bettini, K. J. Bachmann, and J. L. Shay, *J. Appl. Phys.* **49,** 865 (1978).

63. K. J. Bachmann, E. Buehler, J. L. Shay, and S. Wagner, *Appl. Phys. Lett.* **29,** 121 (1976).

64. O. von Roos, *J. Appl. Phys.* **49,** 3510 (1978).

65. W. G. Haines and R. H. Bube, *IEEE Trans. Electron Devices* **ED-27,** 2133 (1980).

66. R. A. Smith, "Semiconductors." Cambridge University Press, London and New York, 1968.
67. P. T. Landsberg, *Solid State Electron.* **18,** 1043 (1975).
68a. M. Wolf, *Proc. IRE* **48,** 1246 (1960).
68b. M. Wolf and M. Prince, *J. Br. IRE* **18,** 583 (1958).
69. A. K. Jonscher, "Principles of Semiconductor Device Operation." Wiley, New York, 1960.
70. W. Van Roosbroeck, *J. Appl. Phys.* **26,** 380 (1955).
71. V. L. Dalal and A. R. Moore, *J. Appl. Phys.* **48,** 1244 (1977).
72. J. G. Fossum and E. L. Burgess, *IEEE Photovolt. Spec. Conf., 12th, Proc.*, p. 737 (1976).
73. F. A. Lindholm, J. G. Fossum, and E. L. Burgess, *Proc. IEEE Photovolt. Spec. Conf., 12th*, p. 33 (1976).
74. N. G. Tarr and D. L. Pulfrey, *Solid-State Electron.* **22,** 265 (1979).
75. A. Rothwarf, *Proc. IEEE Photovolt. Spec. Conf., 13th*, p. 1312 (1978).
76. C-T. Sah, R. N. Noyce, and W. Shockley, Proc. *IRE* **45,** 1228 (1957).
77. W. Shockley and W. T. Read, *Phys. Rev.* **87,** 835 (1952).
78. H. Hovel, *IEEE Photovolt. Spec. Conf., 10th, Proc.*, p. 34 (1973).
79. W. Shockley and H. J. Queisser, *J. Appl. Phys.* **32,** 510 (1961).
80. T. L. Tansley, *in* "Semiconductors and Semimetals." (R. K. Willardson and A. C. Beer, eds.), Vol. 7, p. 294. Academic Press, New York (1971).
81. L. J. Van Ruyven, *in* "Annual Review of Materials Science." (R. A. Huggins, ed.), Vol. 2, p. 501. Annual Reviews, Palo Alto, California (1972).
82. A. G. Milnes and D. L. Feucht, "Heterojunctions and Metal–Semiconductor Junctions." Academic Press, New York (1972).
83. U. Dolega, *Z. Naturforsch.* **18a,** 653 (1963).
84. W. G. Oldham and A. G. Milnes, *Solid State Electron.* **7,** 153 (1964).
85. A. Rothwarf, Int. Workshop on CdS Solar Cells and Other Abrupt Heterojunctions, University of Delaware, May 1975, NSF-RANN AER 75-15858, p. 9.
86. L. Nordheim, *Proc. R. Soc. (London) A* **121,** 626 (1928).
87. H. D. Barber, *Solid State Electron.* **10,** 1039 (1967).
88. C. R. Crowell, *Solid State Electron.* **12,** 55 (1969).
89. W. W. Anderson, *Infrared Phys.* **17,** 147 (1977).
90. R. H. Rediker, S. Stopek, and J. H. R. Ward, *Solid State Electron.* **7,** 621 (1964).
91a. A. R. Riben and D. L. Feucht, *Solid State Electron.* **9,** 1055 (1966).
91b. A. R. Riben and D. L. Feucht, *Int. J. Electron.* **20,** 583 (1966).
92. F. A. Padovani and R. Stratton, *Solid State Electron.* **9,** 695 (1966).
93. C. Y. Chang and S. M. Sze, *Solid State Electron.* **13,** 727 (1970).
94. C. R. Crowell and V. L. Rideout, *Solid State Electron.* **12,** 89 (1969).
95. E. H. Rhoderick, *Inst. Phys. Conf. Ser.* No. **22,** 3 (1974).
96. F. A. Padovani, *in* "Semiconductors and Semimetals." (R. K. Willardson and A. C. Beer, eds.), Vol. 7, Ch. 2, pp. 75–146. Academic Press, New York (1971).
97. T. L. Tansley and S. J. T. Owen, *IEEE Trans. Electron Devices* **ED-23,** 1123 (1976).
98. H. A. Bethe, *MIT Rad. Lab. Rep.* 43-12 (1942).
99. C. R. Crowell and S. M. Sze, *J. Appl. Phys.* **37,** 2683 (1966).
100. G. H. Parker, T. C. McGill, C. A. Mead, and D. Hoffman, *Solid State Electron.* **11,** 201 (1968).
101. W. Schottky, *Naturwissenschaften* **26,** 843 (1938).
102. C. R. Crowell and S. M. Sze, *Solid State Electron.* **9,** 1035 (1966).
103. H. C. Card and E. H. Rhoderick, *J. Phys. D Appl. Phys.* **4,** 1589 (1971).

104a. D. L. Pulfrey, *IEEE Trans. Electron Devices* **ED-23,** 587 (1976).
104b. D. L. Pulfrey, *IEEE Trans. Electron Devices* **ED-25,** 1308 (1978).
105. D. R. Lillington and W. G. Townsend, *Appl. Phys. Lett.* **28,** 98 (1976).
106. H. C. Card and E. S. Yang, *Appl. Phys. Lett.* **29,** 51 (1976).
107. S. J. Fonash, *J. Appl. Phys.* **47,** 3597 (1976).
108a. P. T. Landsberg and C. Klimpke, *Proc. R. Soc.* (*London*) *A* **354,** 101 (1977).
108b. P. T. Landsberg and C. Klimpke, *IEEE Photovolt. Spec. Conf., 13th, Proc.*, p. 665 (1978).
109. R. F. McOuat and D. L. Pulfrey, *J. Appl. Phys.* **47,** 2113 (1976).
110. S. Kar, *Tech. Dig. IEEE Electron Devices Meet. Washington, D.C.*, p. 56A (1977).
111. P. Viktorovitch and G. Kamarinos, *J. Appl. Phys.* **48,** 3060 (1977).
112. M. A. Green, F. D. King, and J. Shewchun, *Solid State Electron.* **17,** 551, 563 (1974).
113. P. de Visschere and H. Pauwels, *Proc. C.E.C. Photovolt. Sol. Energy Conversion Conf., 1st*, p. 330 (1977).
114. J. Shewchun, J. Dubow, A. Myszkowski, and R. Singh, *J. Appl. Phys.* **49,** 855 (1978).
115. M. Wolf, *Proc. Annu. Power Sources Symp., 25th*, p. 120 (1972); reprinted *In* "Solar Cells." Wiley (Interscience), New York, 1976.
116. H. W. Brandhorst, *Jpn. J. Appl. Phys.* **16,** 399 (1977).
117. J. Lindmayer and J. F. Allison, *Comsat Tech. Rev.* **3,** 1 (1973); reprinted *In* "Solar Cells." Wiley (Interscience), New York, 1976.
118. J. Mandelkorn and J. H. Lamneck, Jr., *IEEE Photovolt. Spec. Conf., 9th, Proc.*, p. 66 (1972).
119. H. E. LaBelle, Jr., and A. I. Mlavsky, *Mat. Res. Bull.* **6,** 571 (1971).
120. K. V. Ravi, H. E. Serreze, H. E. Bates, A. D. Morrison, D. N. Jewett, and J. C. T. Ho, *IEEE Photovolt. Spec. Conf., 11th, Proc.*, p. 280 (1975).
121. R. K. Riel, NSF-RANN Workshop, Photovoltaic Conversion of Solr Energy for Terrestrial Applications, Vol. II, Cherry Hill, New Jersey, 1973, NSF-RANN-74-013.
122. R. A. Arndt, J. F. Allison, J. C. Haynos, and A. Meulenberg, Jr., *IEEE Photovol. Spec. Conf., 11th, Proc.*, p. 40 (1975).
123a. H. Fischer and W. Pschunder, *IEEE Photovolt. Spec. Conf., 12th, Proc.*, p. 86 (1976).
123b. H. Fischer, *Photovolt. Sol. Energy Conf. Proc., C.E.C., Luxembourg* (1977).
124. J. Lindmayer, *IEEE Photovolt. Spec. Conf., 13th, Proc.*, p. 1096 (1978).
125. W. A. Anderson, A. E. Delahoy, and R. A. Milano, *J. Appl. Phys.* **45,** 3913 (1974).
126. W. A. Anderson, J. K. Kim, and A. E. Delahoy, *IEEE Trans. Electron Devices* **ED-24,** 453 (1977).
127. E. J. Charlson and J. C. Lien, *J. Appl. Phys.* **46,** 3982 (1975).
128. J. P. Ponpon and P. Siffert, *J. Appl. Phys.* **47,** 3248 (1976).
129. G. C. Salter and R. E. Thomas, *IEEE Photovolt. Spec. Conf., 11th, Proc.*, p. 364 (1975).
130. R. B. Godfrey and M. A. Green, *Appl. Phys. Lett.* **34,** 790 (1979).
131. J. B. Dubow, D. E. Burk, and J. R. Sites, *Appl. Phys. Lett.* **29,** 494 (1976).
132. J. C. Manifacier and L. Szepessy, *Appl. Phys. Lett.* **31,** 459 (1977).
133. A. K. Ghosh, C. Fishman, and T. Feng, *J. Appl. Phys.* **49,** 3490 (1978).
134a. T. R. Nash and R. L. Anderson, *IEEE Trans. Electron Devices* **ED-24,** 468 (1977).
134b. C. Fishman, A. K. Ghosh, and T. Feng, *Sol. Energy Mater.* **1,** 181 (1979).
135. R. C. Chittick, J. H. Alexander, and H. F. Sterling, *J. Electrochem. Soc.* **116,** 77 (1969).
136. D. E. Carlson and C. R. Wronski, *Appl. Phys. Lett.* **28,** 671 (1976).
137. P. G. LeComber and W. E. Spear, *Phys. Rev. Lett.* **25,** 509 (1970).
138. W. E. Spear and P. G. LeComber, *J. Non-Cryst. Solids* **8–10,** 727 (1972).
139. A. K. Molhotra and G. W. Neudeck, *Appl. Phys. Lett.* **28,** 47 (1976).
140. W. E. Spear and P. G. LeComber, *Solid State Commun.* **17,** 1193 (1975).

141. W. E. Spear, P. G. LeComber, S. Kinmond, and M. H. Brodsky, *Appl. Phys. Lett.* **28,** 105 (1976).
142. D. E. Carlson, *IEEE Trans. Electron Devices* **ED-24,** 449 (1977).
143. C. R. Wronski, D. E. Carlson, and R. E. Daniel, *Appl. Phys. Lett.* **29,** 602 (1976).
144a. C. R. Wronski, *IEEE Trans. Electron Devices* **ED-24,** 351 (1977).
144b. Y. Kuwano, M. Ohnishi, H. Nishiwaki, S. Tsuda, H. Shibuya, and S. Nakano, *15th IEEE Photovoltaic Specialists Conf.*, Kissimmee, Florida, May 1981.
145. D. A. Jenny, J. J. Loferski, and P. Rappaport, *Phys. Rev.* **101,** 1208 (1956).
146. A. R. Cobat, M. F. Lamorte, and C. W. McIver, *IRE Trans. Mil. Electron.* **6,** 20 (1962).
147. Zh. I. Alferov, H. M. Andreev, M. B. Kagen, I. I. Protasov, and V. G. Trofim, *Sov. Phys. Semicon.* **4,** 2047 (1971).
148 J. M. Woodall and H. J. Hovel, *Appl. Phys. Lett.* **21,** 379 (1972).
149. J. C-C. Fan and C. O. Bozler, *IEEE Photovolt. Spec. Conf., 13th, Proc.*, p. 953 (1978).
150. L. W. James and R. L Moon, *Appl. Phys. Lett.* **26,** 476 (1975).
151. J. M. Woodall and H. J. Hovel, *Appl. Phys. Lett.* **30,** 492 (1977).
152. R. Sahai, D. D. Edwall, and J. S. Harris, Jr., *IEEE Photovolt. Spec. Conf., 13th, Proc.*, p. 946 (1978).
153. M. Ettenberg and H. Kressel, *J. Appl. Phys.* **47,** 1538 (1976).
154. J. Ewan, R. C. Knechtli, R. Loo, and G. S. Kamath, *IEEE Photovolt. Spec. Conf., 13th, Proc.*, p. 941 (1978).
155. H. Van der Plas, L. W. James, R. L. Moon, and N. J. Nelson, *IEEE Photovolt. Spec. Conf., 13th, Proc.*, p. 934 (1978).
156. R. J. Stirn and Y. C. M. Yeh, *Appl. Phys. Lett.* **27,** 95 (1975).
157. Y. D. Shen and G. L. Pearson, *Sol. Energy Mater.* **2,** 31 (1979).
158. G. Nadjakov *et al.*, *Izv. Bulg. Akad. Nauk.* **4,** 10 (1954).
159. R. Williams and R. H. Bube, *J. Appl. Phys.* **31,** 968 (1960).
160. E. D. Fabricius, *J. Appl. Phys.* **33,** 1597 (1962).
161. H. G. Grimmeiss and R. Memming, *J. Appl. Phys.* **33,** 2217, 3596 (1962).
162. J. Woods and J. A. Champion, *J. Electronic Control* **7,** 243 (1960).
163. D. A. Cusano, *Solid State Electron.* **6,** 217 (1963).
164. P. N. Keating, *J. Phys. Chem. Solids* **24,** 1101 (1963).
165. N. Duc Cuong and J. Blair, *J. Appl. Phys.* **37,** 1660 (1966).
166. E. R. Hill and B. G. Kermidas, *IEEE Trans. Electron Devices* **ED-14,** 22 (1967).
167. B. Selle, W. Ludwig, and R. Mach, *Phys. State Solids* **24,** K145 (1967).
168. A. E. Potter, Jr., and R. L. Schalla, *NASA Tech. Note* NASA TND-3849 (1967).
169. I. V. Egorova, *Sov. Phys. Semicond.* **2,** 226 (1968).
170. R. J. Mytton, *Br. J. Appl. Phys.* **1,** 721 (1968).
171. F. Cabannes, *Compt. Rend.* **246,** 257 (1958).
172. H. Moss, *Proc. Nat. Aeronaut. Electron. Conf.*, p. 47 (1960).
173a. F. A. Shirland and J. R. Hietanen, *Proc. Annu. Power Sources Conf. 19th*, p. 177 (1965).
173b. F. A. Shirland, *Adv. Energy Conv.* **6,** 201 (1966).
174. L. R. Shiozawa, G. A. Sullivan, and F. Augustine, *IEEE Photovolt. Spec. Conf., 7th Proc.*, p. 39 (1968).
175. A. L. Fahrenbruch and R. H. Bube, *J. Appl. Phys.* **45,** 1264 (1974).
176. A. Rothwarf, *CEC Photovolt. Energy Conv. Conf., 2nd, Berlin*, p. 370 (1979).
177. P. F. Lindquist and R. H. Bube, *J. Appl. Phys.* **43,** 2839 (1972).
178. H. W. Schock, G. Gilger, W. H. Bloss, and F. Pfisterer, *Vacuum* **27,** 281 (1977).
179. W. D. Gill and R. H. Bube, *J. Appl. Phys.* **41,** 3731 (1970).
180. R. S. Feigelson, A. N'Diaye, S-Y. Yin, and R. H. Bube, *J. Appl. Phys.* **48,** 3162 (1977).

181. T. L. Hench and R. B. Hall, *CEC Photovolt. Energy Conv. Conf., 2nd, Berlin*, p. 379 (1979).
182. T. A. Chynoweth and R. H. Bube, *J. Appl. Phys.* **51**, 1844 (1980).
183. S. Wagner, J. L. Shay, K. J. Bachmann, and E. Buehler, *Appl. Phys. Lett.* **26**, 229 (1975).
184. J. L. Shay, S. Wagner, K. J. Bachmann, and E. Buehler, *J. Appl. Phys.* **47**, 614 (1976).
185. A. Yoshikawa and Y. Sakai, *Solid State Electron.* **20**, 133 (1977).
186. K. S. Sree Harsha, K. J. Bachmann, P. H. Schmidt, E. G. Spencer, and F. A. Thiel, *Appl. Phys. Lett.* **30**, 645 (1977).
187. K. J. Bachmann, H. Schreiber, Jr., W. R. Sinclair, P. H. Schmidt, F. A. Thiel, E. G. Spencer, G. Pasteur, W. L. Feldmann, and K. Sree Harsha, *J. Appl. Phys.* **50**, 3441 (1979).
188. K. J. Bachmann, T. Bitner, F. A. Thiel, W. R. Sinclair, H. Schreiber, Jr., and P. H. Schmidt, *Sol. Energy Mater.* **1**, 249 (1979).
189. H. M. Manasevit, K. L. Hess, P. D. Dapkus, R. P. Ruth, J. J. Yan, A. G. Campbell, R. E. Johnson, L. A. Moudy, R. H. Bube, L. B. Fabick, A. L. Fahrenbruch, and M.-J. Tsai, *IEEE Photovolt. Spec. Conf., 13th, Proc.*, p. 165 (1978).
190. M.-J. Tsai, A. L. Fahrenbruch, and R. H. Bube, *J. Appl. Phys.* **51**, 2696 (1980).
191. J. Gu, T. Kitahara, S. Fujita, and T. Sakaguchi, *Jpn. J. Appl. Phys.* **14**, 499 (1975).
192. D. Lincot, J. Mimila-Arroyo, R. Triboulet, Y. Marfaing, and M. Barbe, CEC *Photovolt. Sol. Energy Conf., 2nd, Berlin*, p. 424 (1979).
193. J. Mimila-Arroyo, Y. Marfaing, G. Cohen-Solal, and R. Triboulet, *Sol. Energy Matl.* **1**, 171 (1979).
194. M. Chu, A. L. Fahrenbruch, R. H. Bube, and J. F. Gibbons, *J. Appl. Phys.* **49**, 322 (1978).
195. J. P. Ponpon and P. Siffert, *Rev. Phys. Appl.* **12**, 427 (1977).
196. K. W. Mitchell, A. L. Fahrenbruch, and R. H. Bube, *J. Appl. Phys.* **48**, 4365 (1977).
197. K. Yamaguchi, H. Matsumoto, N. Nakayama, and S. Ikegami, *Jpn. J. Appl. Phys.* **15**, 1575 (1976).
198. K. Yamaguchi, N. Nakayama, H. Matsumoto, and S. Ikegami, *Jpn. J. Appl. Phys.* **16**, 1203 (1977).
199. Y. Y. Ma, A. L. Fahrenbruch, and R. H. Bube, *Appl. Phys. Lett.* **30**, 423 (1977).
200. S.-Y. Yin, A. L. Fahrenbruch, and R. H. Bube, *J. Appl. Phys.* **49**, 1294 (1978).
201. N. Nakayama, H. Matsumoto, K. Yamaguchi, S. Ikegami, and Y. Hioki, *Jpn. J. Appl. Phys.* **15**, 2281 (1976).
202. S. Wagner, J. L. Shay, P. Migliorato, and H. M. Kasper, *Appl. Phys. Lett.* **25**, 434 (1974).
203. J. L. Shay, S. Wagner, and H. M. Kasper, *Appl. Phys. Lett.* **27**, 89 (1975).
204. L. L. Kazmerski, F. R. White, and G. K. Morgan, *Appl. Phys. Lett.* **29**, 268 (1976).
205. L. L. Kazmerski, M. S. Ayyagari, and G. A. Sanborn, *J. Appl. Phys.* **46**, 4865 (1975).
206a. L. L. Kazmerski, 2nd Quarter Rep. to NSF-RANN and ERDA, AER-75-19576-A01, April, NSF/AER-75-19576-2.
206b. R. A. Mickelsen, *15th IEEE Photovoltaic Specialists Conf.*, Kissimmee, Florida, May 1981.
207. A. Catalano, V. Dalal, E. A. Fagen, R. B. Hall, J. V. Masi, J. D. Meakin, G. Warfield, and A. M. Barnett, *CEC Photovolt. Sol. Energy Conf., 1st, Proc., Luxembourg*, p. 644 (1977).
208. A. Catalano, M. Bhushan, and P. S. Noyar, Emerging Materials Contractors In-Depth Review Meeting, August 19–21, 1980, SERI, Golden, Colorado.
209. C. Clemen and E. Bucher, *IEEE Photovolt. Spec. Conf., 13th, Proc.*, p. 1255 (1978).
210. S. Wagner and P. M. Bridenbaugh, *J. Cryst. Growth* **39**, 151 (1977).
211. G. H. Chapman, J. Shewchum, B. K. Garside, J. J. Loferski, and R. Beaulieu, *Sol. Energy Mater.* **1**, 451 (1979).
212. M. Schoijet, *Sol. Energy Mater.* **1**, 43 (1979).

213a. R. A. Scranton, J. B. Mooney, J. O. McCaldin, T. C. McGill, and C. A. Mead, *Appl. Phys. Lett.* **29**, 47 (1976).
213b. J. S. Best, J. O. McCaldin, T. C. McGill, C. A. Mead, and J. B. Mooney, *Appl. Phys. Lett.* **29**, 433 (1976).
214. M. J. Cohen and J. S. Harris, Jr., *Tech. Digest IEEE IDEM, Washington, D.C.*, p. 247 (1978).
215. A. Heeger, personal communication, University of Pennsylvania, Philadelphia.
216. C. W. Tang and A. C. Albrecht, *Nature (London)* **254**, 507 (1975); *J. Chem. Phys.* **63**, 953 (1975).
217. D. L. Morel, A. K. Ghosh, T. Feng, E. L. Stogryn, P. E. Purwin, R. F. Shaw, and C. Fishman, *Appl. Phys. Lett.* **32**, 495 (1978).